Se

ADDIS ABABA UNIVERSITY
SCHOOL OF GRADUATE STUDIES

BEHAVIOUR OF LITHIUM ATOMS IN ^{111}In DOPED ZnSe

By

Yared Endalamaw

February 1994

BEHAVIOUR OF LITHIUM ATOMS IN ^{111}In DOPED ZnSe

By
Yared Endalamaw

A Thesis
Submitted in Partial Fulfillment for the Degree Master of Science in Physics in the Addis Ababa University.

February 1994

ADDIS ABABA UNIVERSITY
SCHOOL OF GRADUATE STUDIES

BEHAVIOUR OF LITHIUM ATOMS IN ^{111}In DOPED ZnSe

By

Yared Endalamaw
Department of Physics
Addis Ababa University

Approved by the Examining Board

Dr. F. Dworschak
External Examiner

Dr. I. M. Kashiriski
Advisor

Dr. S.S. Kotelnikov
Examiner

Dr. A.N. Mishin
Examiner

ACKNOWLEDGEMENTS

I feel higly glad to express my deep gratitude to my advisor in Germany, Prof. Dr. Th. Wichert at Technische Physik, Universität des Saarlandes in Saarbrücken with whom I had the pleasure of discussing research results on several round discussions in a conducive atmosphere. Also, I feel quite happy to deliver my gratitude to Mrs. Wichert at this juncture.

I am deeply thankful to my advisor in Ethiopia, Dr. I. M. Kashirsky for his unreserved cooperation in teaching and advising me on many interesting problems.

My special thanks go to R. Lermen with whom I closely exchanged a lot of research experience in Saarbrücken. The cooperation of Dr. H. Wolf in Saarbrücken deserves my appreciation. I benefited a lot from discussions with Th. Filz, U. Hornhauer, Th. Krings, E. Singer, U. Ott, St. Lauer and V. Osthelmer, I deliver my Sincere gratitude to all of them. Also, I feel quite grateful to DAAD (DEUTSCHER AKADEMISCHER AUSTAUSCHDIENST) for offering me a financial support during my study both in Ethiopia and in Germany. Dr. F. Dworschak, from IFF-KFA Jülich in Germany, coordinated my six months research project in Saarbrücken, Germany from which I gained fruitful experiences and which is also the basis of this thesis. I extend my warmest gratitude to him for his remarkable collaboration.

Mrs. I. Michael's cooperation in Saarbrücken was remarkable and I am thankful to it. It is a pleasure to me to thank M. Kahssay, H. Ambaye S. Solomon, and A. Teferra for their valued assistance. Also, I am quite grateful to W/t Shitaye Geremew, Secretary at the Department of Mathematics, A.A.U., for her efficient work.

C O N T E N T S

Abstract

This thesis work focuses at investigating the behaviour of diffused Lithium atoms into the II–VI semiconductor ZnSe doped with the radioactive dopant ^{111}In using the PAC (perturbed $\gamma\gamma$ angular correlation) technique.

The atomistic information about defects surrounding the probe atom can be obtained using this technique.

Inorder to investigate the p–doping problems in ZnSe, PAC experiments were conducted on ZnSe after diffusion with the potential p–type dopant Lithium using the PAC spectroscopy. Obviously, it was found much more difficult to prepare a p–type sample by doping ZnSe with Lithium atoms. The failure of p–doping after doping with Lithium may be associated with the diffusion mechanism which prevents the Lithium atoms from occupying lattice sites in the metal sublattice, a necessary condition for Lithium to act as an acceptor.

However, Lithium induced effects were properly investigated through special experimental treatments and the various dependence of the diffusion of Lithium on the matrix temperature and the vapour pressure of Lithium were noted.

From the PAC experiments, it was observed that Lithium diffusion introduces vacancies in the metal sublattice which are observed by their pairing with the In probe atom. The generation of $In_{Zn} - V_{Zn}$ *pairs is known to occur if both the sample and the Lithium source are held at temperatures exceeding a characteristic value.*

A better understanding of the mechanism of vacancy creation during Li incorporation might also shed new light on the problem of the missing p–type conductivity after Li–diffusion.

Introduction

Wide band gap II–VI compounds of the Zn and Cd chalcogenides.(such as CdS, ZnTe, ZnSe and ZnS) have been of great interest to the scientific community for many years. The potential of these compounds for visible light emitting diode (LED) materials emanates from the excellent luminescent properties they possess and the nature of their high band gaps which range throughout the visible spectrum into the near ultraviolete (UV), producing high efficiency luminescence under UV and electron beam excitation.

Furthermore, II–VI compounds are direct band gap materials and, therefore, an efficient radiative recombination can be achieved in a straight forward manner [1] – i.e., band-to-band transitions since no crystal-momentum-preservation problems exist.

The application of these materials in p–n junction devices, however, has been hampered by the problems encountered in making both conducting n–type or p–type material [1,2].

In order to make efficient blue light emitting devices, considerable effort has been invested in trying to fabricate p-n junctins in the large band gap (~ 2.7 eV) semicnductor ZnSe.Unfortunately, it has proven very difficult to make this material p-type because of apparently unavoidable compensation[3]. Although II–VI compound semiconductors have a long history with regard to their use, the variety of the intrinsic point defects are not known at a high level of accuracy since their identification and their mutual interactions as well as their interactions with impurity atoms still pose a major puzzle[4] However, the failure of making p–n junction devices out of wide band gap semiconductors is attributed to intrinsic point defects. The research work devoted to the investigation of the causes of doping problems in II–VI compounds has been in progress and the role of compensating defects in the doping mechanism is being studied.

The atomistic structure of defects can be studied by employing radioactive atoms which could serve as microscopic probes [5]. The perturbed $\gamma\gamma$ angular correlation technique (PAC) is a nuclear technique that measures the defect specific electric field gradient *tensor (EFG) using the radioactive probe atom like ^{111}In. Employing this technique, it is possible to investigate the formation of probe atom – defect complexes on an atomic scale [6].*

Although ZnSe can easily be made n-type, the strong interaction of intrinsic defects with possible p-dopants in ZnSe leads to the self-compensation phenomena thereby causing a crucial problem in making it p-type.

SinceLithium introduced on the Zn-site is regarded as a promissing candidate for p-doping of ZnSe, this work was devoted to investigate the incorporation of Lithium into ZnSe on an atomic scale. Lithium atoms that occupy the Zn site and act as an acceptor should form coulombic bound pairs with the donors that also exist in the crystal. Such a pairing is easily detectable by the PAC technique using the radio-active donor ^{111}In as a probe atom as has been successfully proven for Si, Ge and several III-V semiconductors [[5,7].

Chapter I deals with the general introduction to II-VI semiconductor compounds and their crystallographic form. As II-VI compounds are optically important, an important aspect of their optical property is discussed in Chapter II. Following this the self compensation phenomena in II-VI compounds is presented.

Chapter III discusses the basic principles of the PAC (Perturbed $\gamma\gamma$ Angular Correlation Technique) as applied to defect studies.

The experimental work, upon which this thesis is developed, is fully presented in Chapter IV. The experiments of diffusing Lithium into ^{111}In doped ZnSe shed light on the possibilities of p-doping ZnSe and understand the challenges. Moreover, the application of special thermal treatments proved to be an efficient method in reducing intrinsic defects, consequently the separate observation of Lithium induced effects was successfully accomplished. A conclusion is drawn by stating the major results and the appendices are devoted to highlight specific subtopics in detail.

CHAPTER I

II-VI Semiconducting Compounds

In this chapter a brief introduction to II-VI semiconductors along with the motivation for the research on compound semiconductors is presented. The varieties in the potential application areas of II-VI compounds are also indicated.

A finishing touch to this chapter comes after presenting the crystallographic forms with which II-VI compounds are characterized.

1.1 General Introduction to II-VI Compounds

II-VI compounds are formed from the combination of the group II and group VI elements of the periodic table. Included in such a broad definition are the oxides, sulphides, selenides and tellurides of Beryllium, Magnesium, Zinc, Cadmium and Mercury [8].

The study on semiconductors has flourished since the research has been extended to the realms of compound semiconductors in addition to studies on the elemental group IV semiconductors. In particular, the increased progress of semiconductor technology in the 1950's exposed the limitations of Silicon and Germanium in connection with the character and magnitude of their forbidden energy gaps.

A remarkable success has been achieved with the compound semiconductors since the research on them has allowed the investigation of different ranges of the energy gaps.

Up to now, systematic studies have been accomplished on II–VI compounds parallel to similar studies in the III–V compounds. The research outcome on II–VI compounds have revealed much more about the general nature of these compounds, in particular the feature of chemical stability at room temperature gained from the higher energy gap characterizing these materials was noted.

A possible motive towards the II–VI compounds comes in the various areas that these compounds are applied. For instance, among the II–VI compounds, CdS and CdSe are highly photoconducting ZnS is strongly luminescent and the compound that is studied in this thesis, ZnSe is a promising candidate for the blue green laser diode if it is P–doped. An optical property of II–VI compounds is studied in Chapter II.

1.2 Crystallographic form

The above mentioned II–VI compounds take one of two crystalline structures, zinc blende and wurtzite, both of which are characterized by tetrahedral lattice sites. In general, the combination of group II and VI elements gives on average four valence electrons per atom; this is a situation conducive to the formation of a tetrahedral lattice site where there is a tendency towards sharing rather than the transfer of electrons between atoms.

A tetrahedral lattice site in a compound AB is one in which each atom A is surrounded symmetrically by four nearest neighbouring B atoms.This is possible when the B atoms sit at the corners of a tetrahedron with the A atom situated at its geometrical centre. As far as their tetrahedral nature is concerned, the A and B sites are identical. The combination of the tetrahedral sites takes the two possible forms shown in fig. 1.1 which are relevant to the compounds of interest.

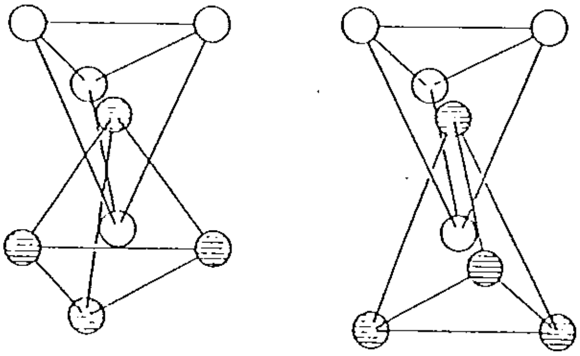

(a) (b)

FIG. 1.1. Tetrahedral sites for a compound. (a) Bases of tetrahedra parallel and in line vertically. (b) Bases of tetrahedra parallel and 60° out of line vertically.

These two combinations of the tetrahedral lattice sites lead to the two crystal structures, wurtzite and zinc blende.

(a) **Wurtzite.** The wurtzite structure which is in the hexagonal crystal class has the combination of tetrahedral sites illustrated in fig. 1.1(a). It consists of two interpenetrating close-packed hexagonal lattices, as illustrated in fig. 1.2 displaced with respect to each other by a distance $\frac{3}{8}$ c along the hexagonal c-axis. For a wurtzite structure with ideal tetrahedral sites, the nearest neighbour distance is $\frac{3}{8}$ c or $\sqrt{\frac{3}{8}}$ a , which yields a c/a ratio of $\sqrt{8/3} = 1.632$.

The II-VI compounds BeO, ZnO, ZnS, CdS, ZnSe, CdSe and MgTe have all been observed to take the wurtzite structure.

(b) **zinc blende.** This structure is derived from the diamond structure and is composed of two interpenetrating cubic close-packed lattices, illustrated in fig. 1.3, translated with respect to each other by 1/4 of the body diagonal. It should be noticed that this structure belongs to the cubic crystal class possessing the combination of tetrahedral sites illustrated in fig. 1.2

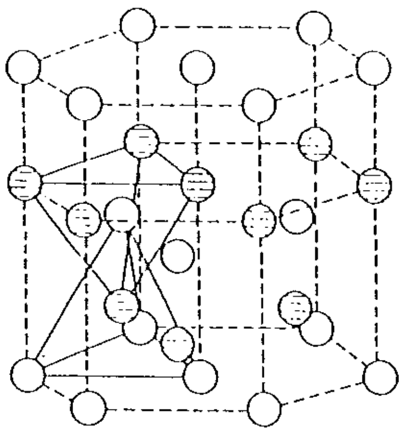

FIG. 1.2. Wurtzite structure, illustrating type (a) tetrahedral site.

The nearest neighbour separation for the Zinc blende structure is easily seen to be $\frac{\sqrt{3}a}{4}$. The sulphides, selenides, and tellurides of Beryllium, Zinc, Cadmium and Mercury have all been obtained with the zinc blende structure.

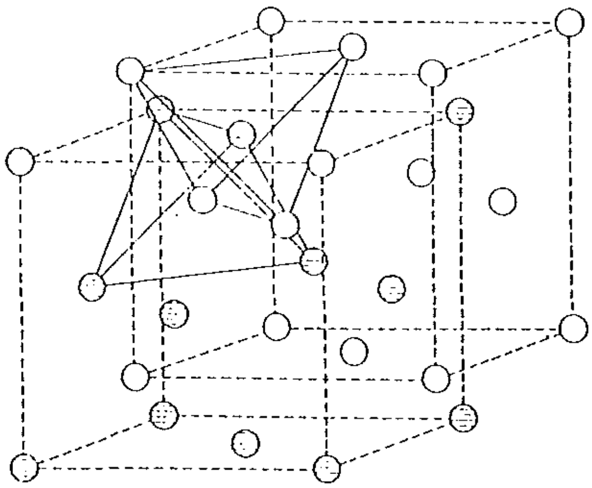

FIG. 1.3. Zinc blende structure, illustrating type (b) tetrahedral site.

CHAPTER II

Properties of II – VI Compounds

In this chapter, the luminescence phenomena in II-VI compounds is discussed to highlight the enormous potentialities possessed by these compounds for optical applications which is mainly attributed to the nature of their band gap.

Moreover, the self compensation phenomenon in II-VI compounds is discussed since it strongly affects the physical properties of such compounds. The aim of impurity doping is also stated and the typical impurities in II-VI compounds are tabulated in table 2.3 together with their state.

2.1 Optical Properties : Luminescence in II-VI compounds

This phenomenon describes the emission of radiation which results when a material, previously stimulated, adjusts itself from an excited to a ground state [8].

The prefix to the word luminescence describes the form of stimulation. Photoluminescence, electroluminescence and thermoluminescence are phenomena pertaining to II-VI compounds. There is a somewhat arbitrary division of luminescent emission with regard to the amount of delay of emission after the excitation. For instance, fluorescence refers to emission which occurs within a microsecond of excitation and phosphorescence to time delays exceeding a microsecond. As most luminescent materials exhibit phosphorescence, the name 'phosphors' is applied to them generally.

A great modification of the luminescent behaviour of II-VI compounds will be realized by the addition of impurities. Impurities added to II-VI compounds are termed to be activators (acceptors) and coactivators (donors). These impurities form deep acceptor levels above the valence band and deep donor levels below the conduction band respectively. Therefore, a thermal release of electrons trapped at these levels is impossible at room temperature, consequently the levels are termed to be electron traps.

In addition to defects created by deliberately added impurities, there always exist in crystals natural defects. These natural defects are usually vacancies at the group II and group VI site and they offer respectively self activation and coactivation for the luminescent II-VI compounds. The metal and chalcogen vacancies behave as double acceptor and double donor impurities respectively.

Fig. 2.1 shows the location of the activator and coactivator levels in the forbidden energy gap and the energy transitions which involve luminescent emission can be represented fundamentally interms of three general models

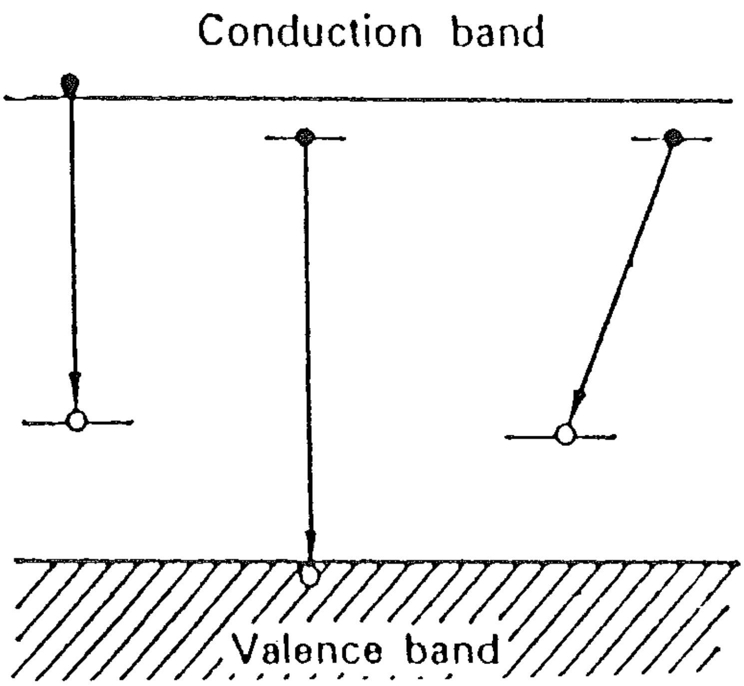

Fig. 2.1 Energy models for luminescent emission in II-VI compounds [8]:
(a) Schön-klasens (b) Lambe-klick (c) Prener-Williams

According to the Schön-Klasens model (a) luminescence is regarded as occuring by a radiative recombination of an electron from the conduction band with a localized acceptor level above the valence band.

The Lambe-klick model (b) explains the luminescent transition via a combination of an electron trapped below the conduction band with a free hole in the valence band. The Prener-Williams model (c) stresses the localized association of activator and coactivator as a possible description of the luminescent emission.

2.2 The Self Compensation Phenomena in II-VI Compounds

Self compensation designates the phenomena of impurity doping limitation attributed to native defects generated in the considered crystal [9]. This phenomenon has been observed in a large number of high band gap semiconductors and among them in several of the II-VI compounds: ZnO, ZnS, ZnSe, CdS, CdSe and CdTe.

A remarkable fact in the self compensation effects is the intercorrelation which exists at high temperature between charged impurities and native defects. Moreover, the various charged species are linked by the condition of electric neutrality.

Various authors [10], [11], [12] have conducted these analyses thereby offering a plausible interpretation of compensation effects in terms of native defect properties: energy of formation and electronic energy levels, which unfortunately cannot be precisely calculated apart from appearing as adjustable parameters.

Although the wide band gap possessed by some semiconductors like ZnSe, ZnS, CdS and CdSe is well suited to optical applications using blue or green light like in semiconductor lasers and light emitting diodes there is a fundamental problem with these materials: some wide band gap materials can easily be made n-type but not p-type [13]. The failure of amphoteric doping (pn junctions) is primarily due to electrical compensation of the intentionally added donor or acceptor impurities by native defect centers of the opposite conductivity type.

According to this mechanism, the wide band gap could promote the formation of compensating native point defects because the formation energy of the defect is recouped by the energy gained when electrons are transferred between the defect's electronic state in the gap and the Fermi level.

As the above notion is expressed in terms of a balance of energies, it should be noted that if the energy required to form defects is large compared to the energy gained by compensation, the compensation of impurity centers by the defects becomes unavoidable [1].

The defect formation energy is a function of both lattice temperature and band gap; in wide band gap materials at elevated temperatures, compensating centers are formed with relative ease. The energy released to the system through compensation is related to the ionization energy of the acceptor center being compensated; therefore the closer the acceptor level is to the valence band, the more easily compensation can occur. For a given material, the probability of self-compensation can, therefore, be minimized by choosing a deep acceptor and introducing it at low temperatures.

There has been considerable experimental evidence to support the premise that compensation by native defect centers is a predominant factor in the failure to achieve amphoteric doping.

However, there are also additional factors that deserve attention: for example, the solubility limit of some otherwise suitable shallow acceptor impurities in sulphides and selenides may be too low for compensation of the donor impurities accidentally introduced during the crystal growth.

There is evidence that some other acceptor impurities such as Li in CdS [14], Ag in CdS [15], and Li in ZnTe [16] may undergo self-compensation by distributing themselves between various impurity states. The dopants may also form electrically and optically inactive complexes with impurities or native defects unintentionally introduced or created in the material during the growth process.

It was noted that most II–VI compounds contain a high concentration of interstitial metal and chalcogen atoms. Such interstitial defects have not been demonstrated to exhibit electrical activity at room temperature, but it is conceivable that the interaction of these interstitials with dopants during diffusion may result in the formation of stable neutral centers. These may occur in the form of atomically dispersed complexes, precipitated second phases which extract the added impurities, or electrically active compensating centers [17].

For the II– VI semiconducting compound studied in this thesis, ZnSe (E_g ~ 2.7eV) p-type doping is quite difficult. This may be understood by the self compensation phenomena due to defects that introduce electrons in levels near the conduction band. The spontaneous formation of native defects would thus prevent the Fermi level from moving below a fixed value that is determined by the formation energies and electronic levels of native defects, independent of the dopant and the growth method used. It should be noted here that compensating defects play a preliminary role in affecting the electronic state density in the band gap of a wide band gap semiconductor under investigation, which brings about significant changes of the position of the Fermi level that could have characterized a particular type of doping otherwise.

This argument is very impressive. It would explain why the difficulty in producing p-type(or n-type) material, is universal, appearing for all growth and doping techniques, and for all dopants. Also, the same analysis describes why doping problems occur less severely in medium gap materials such as CdTe (E_g = 1.5eV) which can be made in both low-resistivity n and p-type form.

Whether the native defects with the lowest formation energy are donors or acceptors could be well understood from the type of doping, n–doping or p–doping, that causes more difficulty in a considered II–VI semiconducting compound.

For instance, according to the suggestion of Jansen and Sankey [18], the native defect mechanism can account for the difference between ZnSe, which can be made n-type, and ZnTe, which can be made p-type, eventhough it is impressively noticed that both materials have striking similarities in other physical properties, like in their crystal structure, lattice constant, and thermal expansion coefficients.

Large concentrations of native defects could be generated if there exist stochiometric deviations, however undetectably small they are Nevertheless, it is found that the defects formed depend on whether the sample is n-type or p-type, but they always compensate. Hence deviations from stochiometry cannot explain why ZnSe can be doped n-type but not p-type, because their compensational role stands on equal footing for both n-type and p-type materials as well.

Therefore, potential dopants need to be examined case by case inorder to understand the specific mechanism for the compensation. This approach is quite fruitful as it could shed light in understanding the possible states in which the doped impurity exists in the considered crystal.

2.3 Impurity Doping

Impurities are incorporated into semiconductors in order to achieve electrically and optically active centers [1].

Table 2.3 shows some of the well-known donor and acceptor impurities in II-VI compounds in which consideration is given to substitutional metal or chalcognide sites.

Usually, relations are established between the ionization level at a particular sublattice site with the radius of the site; specifically, deep centers are obtained from the larger potential metal and chalcogenide sites. The behaviour of possible dopants from group III such as Al, Ga and In is properly investigated - they substitute for Zn or Cd and act as donors. In CdS (E_g=2.38eV) low-resistivity n-type samples can be prepared by doping with these elements, achievement being realized with little difficulty.

As far as the II-VI Zn compounds are concerned, these donors are largely compensated by Zn vacancies, and as- grown bulk materials exhibit high resistivity.

Moreover, the halogen donors (F,Cl,Br,I) play similar roles to that of group III donors in that the halogen donors form a defect complex by associating themselves with a Zn or Cd vacancy.

The group IA elements (e.g. Li, Na) are expected to act as p-type impurities when they occupy the metal substitutional site. If introduced on the Zn site, Li acts as a potential p-dopant and investigating the possibilities and challenges along this line was the central theme of this thesis work. The detailed outcome is fully discussed in chapter IV from which the behaviour of the diffusant Lithium atoms in ^{111}In doped ZnSe is experimentally studied under well defined experimental conditions.

Table 2.3 Donor and acceptor impurities in II-VI compounds [1]

Group	Impurity	Sub-for	Donor	Acceptor
IIIA	B,Al,Ga,In,Tl	Zn, Cd	D	
VIIA	F, Cl, Br, I	S, Se, Te	D	
IA	Li, Na	Zn, Cd		A
IB	Cu, Ag, Au	Zn, Cd		A
VA	N, P, As, Sb, Bi	S, Se, Te		A

Group IB (Cu, Ag, and Au) elements are known to diffuse extremely rapidly as interstitials, but they can also be incorporated in the lattice as substitutes for Zn or Cd .Although in most cases these elements form complexes with native defects or other impurities, they may also be incorporated as isolated substitutional acceptors in Zn chalcogenides.

CHAPTER III

The Perturbed $\gamma\gamma$ Angular Correlation Technique

As a powerful nuclear technique for the microscopic investigation of solid state properties, the perturbed $\gamma\gamma$ angular correlation technique makes use of the hyperfine interaction between a nuclear moment-magentic dipole or electric quadrupole of a nuclear probe atom and internal electromagnetic fields within the solid[21].

The technique was originally developed and applied to the determination of magnetic dipole and electric quadrupole moments of excited nuclear states[19]. Today, the precise determination of electromagnetic field gradients in the local environment of radioactive probes constitutes the main application of this nuclear method.

3.1 Theory on the $\gamma\gamma$ angular correlation technique

The central concept behind the angular correlation technique originates from the fact that the probability of photon emission from a radioactive nucleus generally depends upon the angle between the nuclear spin axis and the direction of emission.

Attributed to the normal random orientation of nuclear spin, the radiation from a radioactive sample is isotropic. However, in a situation where there exist an ensemble of nuclei whose spins are not randomly oriented, the radiation pattern will be quite anisotropic. To realize the anisotropicity of the radiation, external factors like low temperature and strong electromagnetic fields can be applied on the sample thereby polarizing or aligning the nuclear spins, as it is the case, e.g. in nuclear magnetic resonance (NMR).

The method for spin alignment used by the angular correlation technique is accomplished by selecting only those nuclei whose spins are directed in a preferred direction. In a successive emission of two γ-rays, the preferred spin direction is fixed by the direction of observation of the first γ-ray and from the knowledge of this direction a selection of an ensemble of similarly aligned nuclear spins can be made. In doing so, we also fix the direction of observation of the second γ-ray and consequently the correlated second γ-quantum of the cascade displays an anisotropic radiation pattern.

The anisotropic radiation pattern rotates in response to the hyperfine interaction taking place between the nuclear spins and the electromagnetic field gradients within the lattice. The precession of the nuclear spins caused by this interaction is characterized with typical precession frequency "ω".

The schematic diagram in fig. 3.1 depicts the basicprinciples of a perturbed $\gamma\gamma$ angular correlation (PAC) experiment [19].

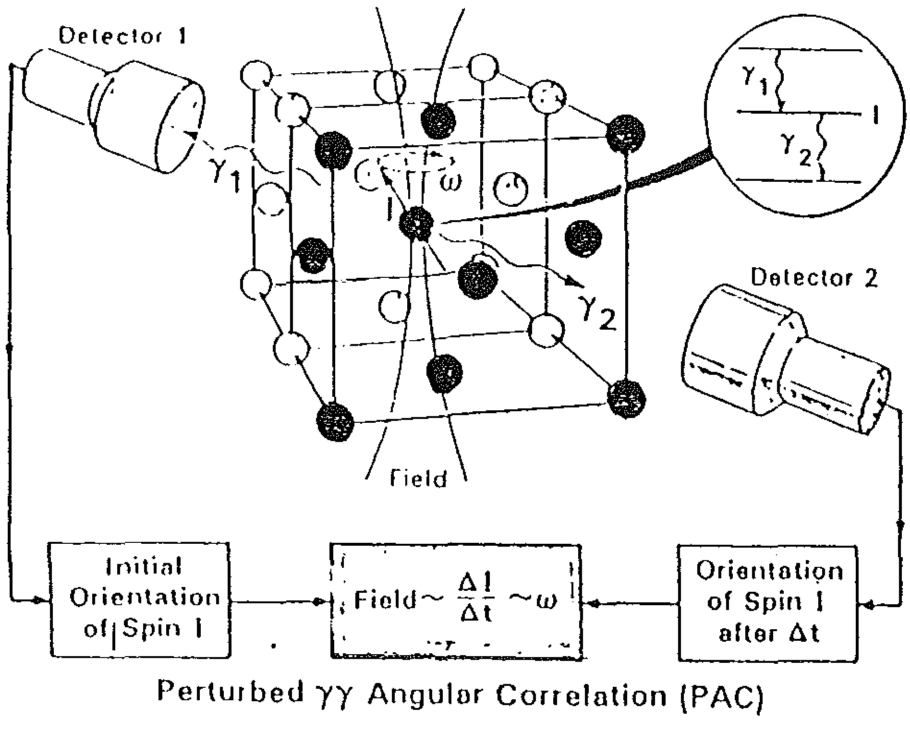

Fig. 3.1 In a PAC experiment, the local field at the site of a radioactive probe atom induces a precession of the probe atom's spin $\vec{I}$. The probability to detect γ_1 and γ_2 in coincidence is modulated by the precession frequency ω as the directions of the photons are coupled to the instantaneous spin orientation[19].

As it is obvious from the above figure, the electromagnetic field inside the sample is detected by a radioactive probe atom, as the probe atom's nuclear spin $\vec{I}$ precesses due to its hyperfine interaction with the electromagnetic field. This phenomenon is common to other PAC isotopes as well.

The radioactive probe atom will be excited by an electron capture process and consequently it leaves this excited state by emitting two photons, γ_1 and γ_2. The spatial emission probability of the two γ-rays will be controlled by the instantaneous orientations of the nuclear spin $\vec{I}$ during the emission times $t_1 = 0$ for γ_1 and t_2 for γ_2. Hence, the experimentalist knows the initial orientation of $\vec{I}$ and the new spin orientation after the time $\Delta t = t_2 - t_1$ respectively from detectors 1 and 2.

The change in the spin orientation, $\Delta\vec{I}$ as reflected by the $\gamma\gamma$ coincidence probability has to be observable for a range of Δt values that is comparable with at least one full revolution of the nuclear spin [5].

In order to get the necessary range of Δt values, the nuclear isomeric state with spin $\vec{I}$ and electric quadrupole moment Q has to posses an adequate life time τ. Moreover, from the relative spin orientation $\Delta\vec{I}$ per time interval Δt, information can be extracted about the spin precession frequency, ω. Besides, it should be noted that the spin precession frequency characterizes the state of the sample.

During the emission of the γ-rays, the respective angular distribution of the emitted γ-rays and the orientation of the resulting nuclear spin are directed in accordance with the validity of the conservation of angular momentum of the system (i.e. the nucleus and the emitted γ-rays). It should be noted that the successive detection of a 2-photon cascade allows a direct observation of the change in spin orientation during the time interval between the emission of the γ-rays, thereby estabilishing the precession frequency ω. At this juncture, it must be attentively noted that the spin precession frequency ω is established by considering the decay of a statistical ensemble of probe atoms within the host crystal.

What information can be gained about microscopic solid state properties by employing the PAC technique?

Using PAC, full information concerning the number of different internal fields and their strengths, acting on probe atoms, is transmitted by the frequency modulated radiation field.

In PAC experiments, at the site of a nucleus, the hyperfine interaction of electromagnetic fields with a nuclear moment is observed. The hyperfine interaction causes the energy shift of the nuclear states and it is describable interms of the corresponding Hamiltonian expressing this shift in energy.

As is contained in eq.(1) below, the interaction part of the Hamiltonian is composed of a magnetic and electric part[21].

$$\mathcal{H} = \mathcal{H}_{mag} + \mathcal{H}_{el} \tag{1}$$

The first term in eq.(1) describes the magnetic part of the interaction at a nucleus with spin $\vec{I}$ and magnetic moment $\vec{\mu} = \gamma_n \hbar \vec{I}$. It consists of the nuclear Zeeman term, caused by a magnetic field $\vec{H}$, and the hyperfine coupling between $\vec{I}$ and the electron spin $\vec{S}$, look eq.(2) below

$$\mathcal{H}_{mag} = -\gamma_n \hbar \vec{H}\cdot\vec{I} + A \vec{I}\cdot\vec{S} \tag{2}$$

where $\gamma_n = g\mu_N/\hbar$ (g:nuclear g factor; μ_N: nuclear magneton) and A is the magnetic hyperfine coupling constant.

The second term in eq.(1) arises from the interaction between the nuclear electric charge distribution and the charge distribution of the surrounding electrons and positive ions. From this part of the hyperfine interaction, information is obtained about electric charge distribution around the probe nucleus.

3.2 The Electric Field Gradient as measured by PAC

Defects, like intrinsic lattice defects or impurity atoms manifest themselves by creating a typical electric field gradient (EFG) at the sites of the neighbouring lattice atoms.

The EFG, which is used for the characterization of a defect on an atomic scale, is the second derivative of the electrostatic potential. The nine components of the traceless tensor describing the EFG are:

$$V_{ij} = \frac{\partial^2 V(r)}{\partial x_i \partial x_j} \qquad (3)$$

It should be noted from eq.(3) that the presence of a defect causes a redistribution of the electronic density which then effects changes in the values of V(r) that then appear as a gradient in the electric field (EFG).

In its principal axis system, the diagonalized EFG tensor is described by the three components V_{xx}, V_{yy} and V_{zz} with the convention

$$|V_{xx}| \le |V_{yy}| \le |V_{zz}| \qquad (4)$$

Moreover, the three diagonal elements satisfy the Poisson equation

$$V_{xx} + V_{yy} + V_{zz} = 0 \qquad (5)$$

From the tracelessness of the EFG tensor, it is evident that two components are sufficient for its complete description.

Usually chosen are the largest component V_{zz} and the asymmetry parameter η, which is defined as

$$\eta = \frac{V_{xx} - V_{yy}}{V_{zz}} \qquad (6)$$

Attributed to the convention in eq.(4), the values of η lie in the range from 0 to 1, where η = 0 describes an EFG tensor with axial symmetry.

The strength of the EFG tensor as measured at the site of the probe atom is expressed by the nuclear quadrupole coupling constant

$$\nu_Q = \frac{eQV_{zz}}{h} \tag{7}$$

where Q is the quadrupole moment and V_{zz} the largest of the three components of the EFG tensor in its principal axes system.

The existence of the nuclear quadrupole moment Q along with V_{zz} in (7) above is a consequence of the quadrupolar part of the electrical hyperfine interaction from which information is extracted about lattice defects surrounding the probe atom. The strength of this interaction is proportional to the magnitude of V_{zz}. The coupling constant, measured with a precision of about 1MHZ, and the asymmetry parameter η guarantee the unique tagging of the respective environment of the probe atom giving rise for the measured EFG [5].

Since $V(r) \sim 1/r$ in eq.(3), the strength of the EFG falls with the third power of the distance between the source of the EFG and the probe's site requiring that an observable source has to be located in the immediate neighbourhood of the probe atom.

A defect occupying a substitutional or interstitial lattice site perturbs the original 'defect free' electron density and correspondingly this defect is characterized by an EFG, which is termed to be the 'finger print' of the defect. Indeed, the strength of the perturbation of the original electronic charge distribution by the defect is contained in the magnitude of the coupling constant ν_Q and the parameter η refelcts the symmetery of the formed probe atom - defect complex. Similarly, the orientation of the complex is reflected by the orientation of the EFG tensor's principal axes system; both are described with respect to the host lattice.

In general, an unambiguous characterization and identification of a particular probe atom-defect complex will be achieved by completely specifying the components of the traceless EFG tensor which is the finger print of the defect.

3.3 Spin Alignment

A proper understanding of how the orientation of a nuclear spin can be monitored via the detection of the emitted γ-radiation will be realized by recalling two phenomena:

The conservation of angular momentum, and the angular distribution of electromagnetic radiation with respect to its angular momentum vector $\vec{L}$ [19].

It is well known from the latter point that electromagnetic radiation is transversely polarized or using the particle picture, the photon as a massless particle never has its angular momentum vector, $\vec{L}$ pointing perpendicular to its flight direction $\vec{P}_\gamma$.

Let's consider a photon with angular momentum L = 1 .where the two angular distributions of the γ-radiation are displayed in fig 3.2. The angular distributions show the probability to find a photon along the direction $\vec{P}_\gamma$ enclosing an angle θ with the quantization axis.

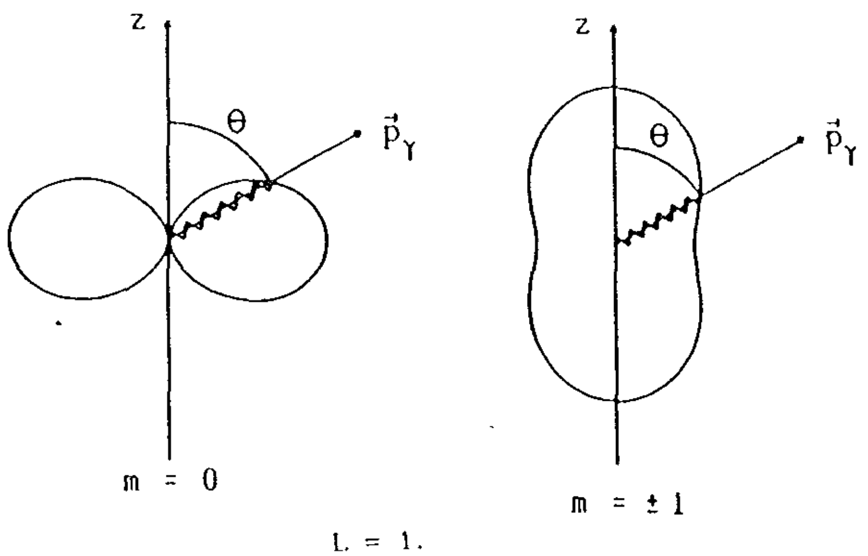

Fig. 3.2 Angular distribution of γ-radition with angular momentum L =1

Notice that m = 0 and m = ±1 refer to photons having their angular momentum vector $\vec{L}$ perpendicular and parallel to the Z-axis respectively. It is obvious from the above angular distribution that the probability to find a photon in Z direction is zero for m = 0.

In light of the conservation of angular momentum, information about the orientation of the nuclear spin $\vec{I}$ can be extracted from the relationship between the direction $\vec{L}$ and the flight direction $\vec{P}_\gamma$.

In order to illustrate this, for an isotope ${}^{A}_{Z}X$ (A: mass number, Z: atomic number) different states of its nucleus are sketched in fig. 3.3 where each state is characterized by its exitation energy E and angular momentum $\vec{I}$. Suppose that the nucleus is produced via the β-decay of a mother isotope ${}^{A}_{Z+1}X$ in its exited state E_i with $\vec{I}_i = 0$.

In order to reach to its ground state E_f the nucleus can lose its energy by emitting a $\gamma\gamma$ cascade consisting of two photons with energies $E_{\gamma 1} = E_i - E$ and $E_{\gamma 2} = E - E_f$. Hence, an unambiguous detection of γ_1 and γ_2 is guaranteed from their different energies: $E_{\gamma 1}$ and $E_{\gamma 2}$. This decay scheme is a prerequisite for PAC.

Moreover, the validity of the conservation of angular momentum for the entire system, that is the nucleus and the emitted γ radiation implies (8) below

$$\vec{I}_i = \vec{I} + \vec{L}_1 \tag{8}$$

where $\vec{I}_i$ is the spin of the initial (excited nuclear state, $\vec{I}$ the spin of the intermediate state and $\vec{L}_1$, the angular momentum of the emitted photon (γ_1).

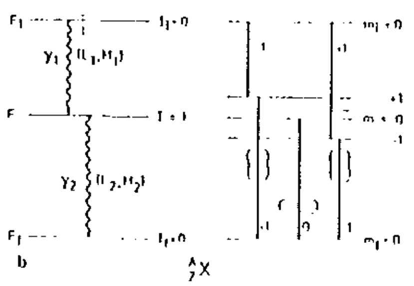

Fig. 3.3 Energies and quantum numbers describing the level scheme of a nucleus that emits a γ_1-γ_2 cascade.

For the corresponding projections onto the quantization axis (Z-axis), we have

$$m_1 = m + M_1 \qquad (9)$$

Thus, it is clear from (8) that the first photon has to carry the spin $L_1 = 1$, since $I_1 = 0$ and the intermediate state of energy E has $I = 1$.

Similar relations hold for the second transition:

$$\vec{I} = \vec{I}_f + \vec{L}_2 \qquad (10)$$

$$m = m_f + M_2 \qquad (11)$$

Choosing the momentum direction $P_{\gamma 1}$ of the photon as quantization axis, only photon states are possible with $M_1 = \pm 1$. With this restriction, it is obvious from (9) that m = 1 since $m_1 = 0$. As a result, the state m = 0 cannot be populated by this transition. Hence, by observing γ_1 along the chosen direction (the quantization axis) a selection of an aligned subensemble in the same direction is observed. That means, the alignment of nuclear spins is granted from the detection of γ_1 and this is the basic spin alignment concept underlying the PAC technique. It should be observed here that the spin alignment is accomplished not by application of external fields and lowering the temerature of the radioactive sample but only by selecting a nuclear subensemble whose spins are oriented in a preferred direction (direction of the detector).

Similarly the second γ radiation (γ_2)will generally show an anisotropic intensity distribution if the γ_1 and γ_2 quanta are measured in coincidence. In fact, the consequence of the spin alignment produced by γ_1 is studied from the second γ-transition. As it is implied from eq.(10) L_2, the angular momentum of γ_2 must equal to 1 since γ_2 connects the nuclear states with spin I = 1 and $I_f = 0$

As shown in fig. 3.4, it seems at first that no restriction exists regarding M_2 since a second detector can be placed at any angle θ to the quantization axis, and without a coincidence with γ_1 a superposition of both radiation patterns shown in fig. 3.2 should be observed which may appear to lead to a 'constant' or isotropic detection probability of γ_2 for all angles θ.

However, because of the preceeding detection of γ_1 a decay fromthe state with m = 0 can not occur and from eq.(11) the photon γ_2 is restricted to $M_2 = \pm 1$ with the consequence that the γ_2 photon displays the radiation pattern shown in fig. 3.2. Eventually, the probability $W(\theta)$ to detect γ_2 at an angle θ with respect to $\vec{P}_{\gamma 1}$ and in coincidence with γ_1 becomes anisotropic and depends on the angle θ.

It should be noticed that the angular correlation between the two γ radiations γ_1 and γ_2 holds only if the two γ-quanta originate from the same decaying nucleus. Once a γ_1 quantum has been registered in the first detector, one will try to detect the second γ quantum only for a time interval corresponding to several times the lifetime τ_N of the intermediate state. The probability that another nucleus decays within this time should be minimized, employing a radioactive source of sufficiently low activity so as to eliminate accidental coincidences: γ_1 and γ_2 originating from two different nuclear decays which are of course uncorrelated.

As is sketched in fig. 3.4 the angular correlation $W(\theta)$ between γ_1 and γ_2 shows a $\cos^2\theta$ or $\cos 2\theta$ dependence when the angle θ between the two detectors is varied, hence it can be calculated that [20]

$$W(\theta) \sim \frac{1}{2}(1 + \cos^2\theta) \tag{12}$$

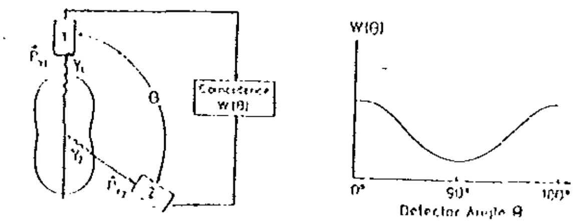

Fig. 3.4 Schematic arrangement of two γ-detectors for a $\gamma\gamma$ angular correlation.

In general, for a spin sequence $I_i \longrightarrow I \longrightarrow I_f$ the angular correlation is described by

$$W(\theta) = 1 + \sum_{k=2}^{k_{max}} A_{kk} P_k(\cos\theta) \qquad (13)$$

where k = 2,4, ... and $\frac{k_{max}}{2}$ is determined by the smallest of the three angular momenta I, L_1 and L_2 which implies that an anisotropic radiation pattern requires $I \geq 1$.

In eq.(13) above, the deviation of the coincidence probability from the isotropic case $W(\theta) = 1$ is described by the angular coefficients A_{kk} whose values can be positive, negative or zero and are governed by the spin sequence and the multipolarity of the γ radiation. Also, note that the existence of the two indices in the angular coefficients is an effect of the $\gamma\gamma$ cascade that involves two γ transitions. As a result it can be formulated as a product of two factors, $A_{kk} = A_k(1)$ $A_k(2)$, one for each transition.

It is evident that corresponding to the increasing angular momentum of the emitted γ ray, the transition probability between nuclear states decreases and consequently we consider cases with L = 1 or 2 so that k_{max} doesn't exceed 4. For the spin sequence 0–1–0 dealt above (k_{max} = 2) and employing the identity $P_2(\cos\theta) = (3\cos^2\theta-1)/2$ together with eqs.(12) and (13) can be rewritten as

$$W(\theta) = 1 + 0.5P_2(\cos\theta) \qquad (14)$$

From eq.(14) we obtain the angular correlation coefficient A_{22} = 0.5.

The above mentioned process is called to be an unperturbed $\gamma\gamma$ angular correlation and it is well-known in nuclear physics. This situation is characterized with a constant population of the m-states created by γ_1 until the emission of γ_2. As a result, the qualifier "unperturbed" enters in defining the phenomena.

In the presence of an extranuclear magnetic or electric field, however this population is perturbed yielding a perturbed $\gamma\gamma$ angular correlation, a process labelled by the letters PAC. Subsequently, there is a change in the angular correlation function $W(\theta)$ and from this change the presence of the perturbing fields will be noticed.

3.4 Spin Precession

In classical theory, a field present at the site of the probe atom will exert a torque on the nuclear spin resulting in a precession of the nuclear spin about the field direction with a Larmor frequency which is proportional to the strength of the field [19].

Hence, from the frequency of the rotating aligned spins information can be obtained about the strength and direction of magnetic fields and similarly behaving electric field gradients as well.

However, it should be noted that the spin precession will be observed through an angle $\Delta\theta$ only if the emission of γ_2 is delayed by a time $\Delta t = \Delta\theta/\omega$ with respect to γ_1. This requires the existence of a mean life time τ characterizing the intermediate nuclear state.

In the absence of magnetic fields and electric field gradients there will be no precession and the probability to detect γ_2 at a time t after γ_1 becomes

$$I(\theta,t) = I_0 e^{-t/\tau} W(\theta) \tag{15}$$

At $t = 0$, the coincidence probability is given by $W(\theta)$ times a normalization constant I_0 whose value is determined by the number of radioactive decays per second, the solid angle subtended by both detectors and the detection efficiency.

For times t' exceeding zero, the spin alignment doesn't change; however because of the finite life time τ of the intermediate state, the coincidence probability decays exponentially with time.

In the presence of a magnetic field or an electric field gradient at the nucleus, however the above situation changes and $W(\theta)$ becomes time dependent as a result of which eq.(15) reads

$$I(\theta,t) = I_0 e^{-t/\tau} W(\theta,t) \tag{16}$$

The fact contained in the above equation is understandable Since the aligned spins $\vec{I}$ start to precess about the field direction immediately after the emission of γ_1. Since the projection of the spins onto the field direction remains constant, the spin precessions will become visible by projecting the spins onto a plane perpendicular to the field direction from which the rotation of the spin alignment with angular frequency ω will be noted. Hence, the spins are rotated by $\theta' = \omega t'$ after a time t' thereby changing θ to $\theta - \omega t'$. This transformation can be preformed for every time t so that the time dependent angular correlation function $W(\theta,t)$ can be formulated as

$$W(\theta,t) = 1 + \sum_k A_{kk} P_k(\cos[\theta - \omega t]) \tag{17}$$

Thus, the angular correlation, observed by two detectors under a fixed angle θ, but as a function of time, oscillates as shown in fig. 3.4.

Note that the coefficients A_{kk} determine the amplitude of the oscillation. Moreover, the observed angular correlation is strongly influenced by the field direction that affects the angular distribution of the radiation pattern emitted by γ_2.

In fact from the sensitivity of the angular correlation function $W(\theta,t)$ on the spatial orientation of the field, enough information can be obtained about the direction of a field inside the lattice of a sample under investigation.

3.5 The PAC time spectrum

Defects at the site of a probe atom are studied from their characteristic finger print, EFG eq.(3). This inference could be achieved from the PAC time spectrum R(t) defined in eq.(18).

In the conducted experiments, the radioactive probe atom ^{111}In is employed. This probe atom decays with a half life of 2.8 days to an excited state of the daughter nucleus ^{111}Cd.

From this excited state successively two γ-rays are emitted encompassing an isomeric state with a half life of 85nS (Look fig.3.5) The interaction between the quadrupole moment Q of the isomeric state and an external EFG generates three frequencies ω_1, ω_2 and ω_3 in the PAC time spectrum sketched in fig. 3.6. Quantitatively it is described by [23]

$$R(t) = A_{22}\left[f\left(S_o + \sum_{n=1}^{3} S_n \cos \omega_n t\right) + (1 - f)\right] \qquad (18)$$

This spectrum is obtained by measuring the coincidence rate of the two emitted γ-rays as a function of the time which passed during the detection of both γ-rays.

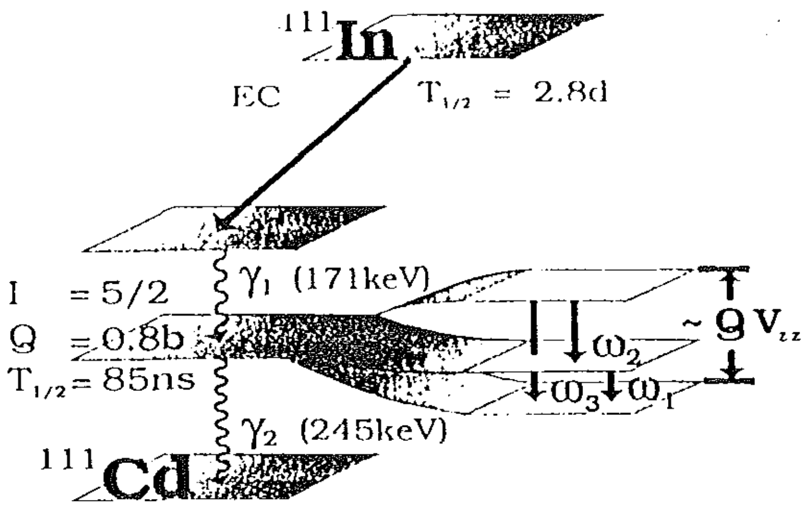

Figure 3.5 Decay Scheme of the radioactive probe atom $^{111}In/^{111}Cd$

The different components V_{ii} of the traceless EFG tensor are obtained from the frequencies ω_n. The largest component V_{zz} is usually expressed by the coupling constant $\nu_Q = \frac{eQV_{zz}}{h}$ which is proportional to ω_1. The asymmetry parameter eq (6) is used as a second parameter and it is deduced from the frequency ratio ω_2/ω_1. The coefficients S_o and S_n depend on the orientation of the EFG tensor with respect to the host lattice, i.e. on the orientation of the formed ^{111}In - defect complex.

The relative fraction of probe atoms associated with the defect that is characterized by this EFG enters via the parameter

$$f = \frac{[\mathrm{In} - \mathrm{defect}]}{[\mathrm{In}]} \qquad (19)$$

and accordingly, the term (1-f) describes the fraction of In atoms without a defect. Thus, using the local concentration of In atoms [In] the concentration of [In - defect] complexes can be determined directly.

As it is clear from fig. 3.6, three frequencies ω_1, ω_2 and ω_3 are observed from which the magnitude of ν_Q eq.(7) and the asymmetry parameter η eq.(6) of the EFG are determined; from their amplitudes the orientation of the EFG tensor is obtained and the fraction of probe atoms that is associated with the defect giving rise to this EFG.

3.6 Experimental Set up

It is obvious from eq(16) that at least two detectors are necessary to measure the angular correlation between γ_1 and γ_2 as a function of time elapsed between the arrival of both γ-rays. The principles of the γ-ray detection can be discussed in refrence to the schematic diagram in fig. 3.7.

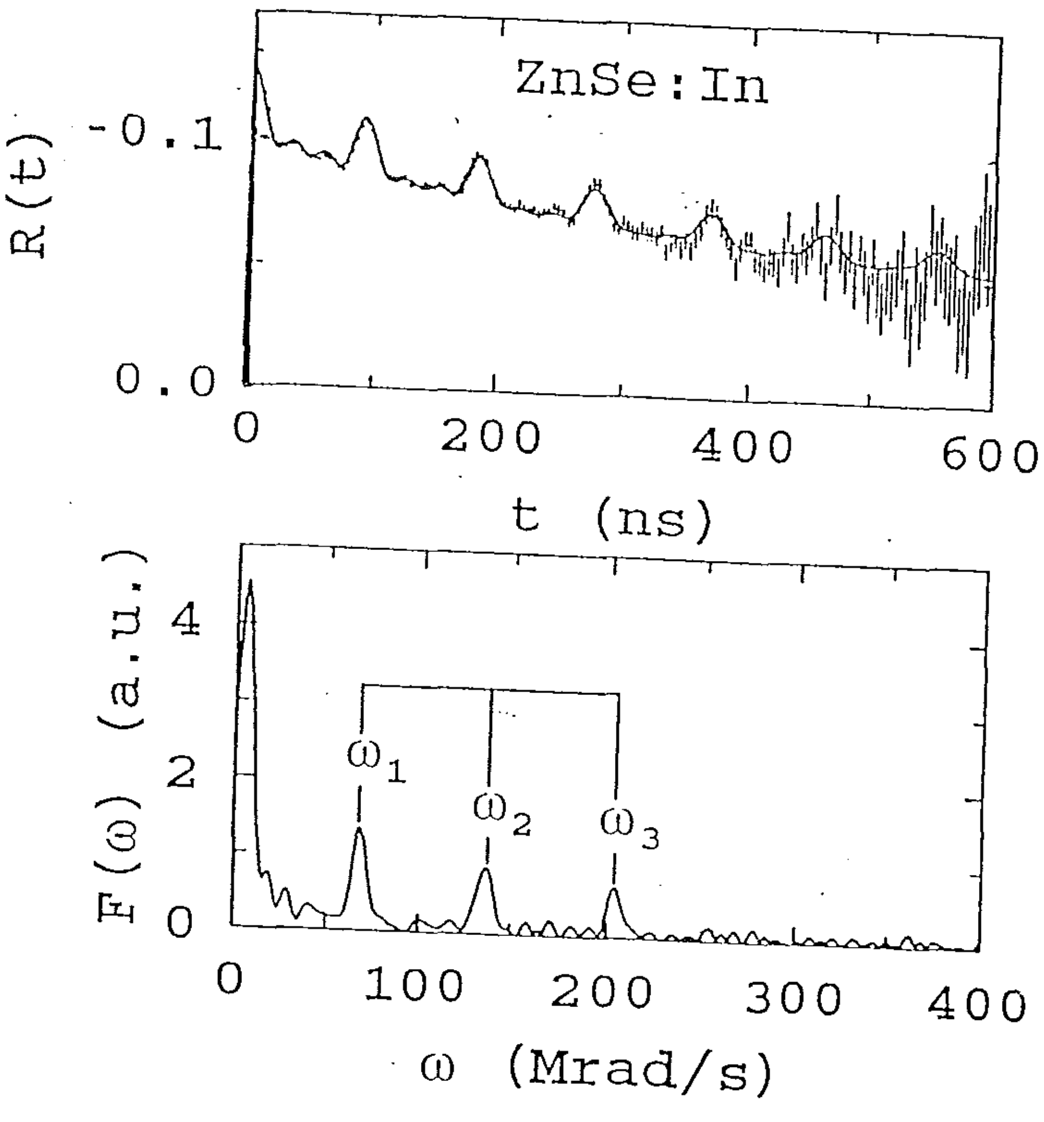

Fig. 3.6 PAC time spectrum and its Fourier transform $F(\omega)$ [6]

Using the electronic set up (fig. 3.7), it is possible to analyze the energy E_γ and the arrival time t_γ for each detected γ-ray. As γ-detectors, NaI(Tl) or BaF_2 crystals coupled to a photomultiplier, are used; these have a time resolution of about 1nS, an energy resolution of about 10% and accept counting rates up to $10^5 S^{-1}$.

Fig. 3.7 shows the main elements of an angular correlation set up. Detector 1 is tuned to record the first γ-quantum of the $\gamma\gamma$ cascade, and detector 2, to record the second one. After conversion of the γ-radiation into a light flash (crystal), which subsequently produces an electron avalanche (photomultiplier), the resulting voltage pulse is split into two signals, E_γ, t_γ , and amplified [21].

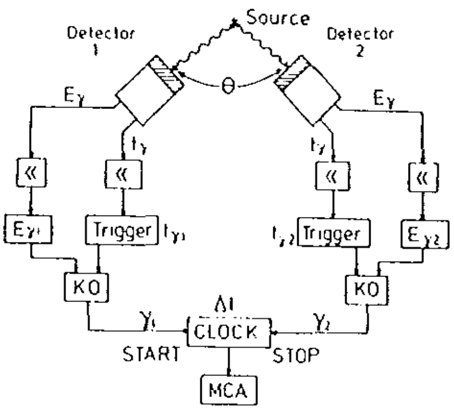

Fig3.7. Electronic setup for recording a γ-γ angular correlation spectrum. <<: amplifier: E_γ: single channel analyzer; Trigger: constant fraction discriminator; KO: coincidence; CLOCK: time-to-pulse-height-converter; MCA: multichannel analyzer for storage of the γ-γ angular correlation spectrum.

In this way, a slow energy signal E_γ with good energy resolution and a fast time signal t_γ with a fast, jitter-free pulse rise time are formed. The trigger creates a digital pulse which defines the arrival time of the respective γ-ray.

After the amplification, a slow energy signal E_γ possessing a good energy resolution and a fast time signal t_γ with a fast, jitter- free pulse rise time are formed. The arrival time of the respective γ-ray is well-defined from a digital pulse created by the trigger. The passage of the energy signal through the energy analyzer will take place only if the energy matches the preselected value of $E\gamma_1$ (detector 1) or $E\gamma_2$ (detector 2).

The digital output signals of the energy analyzers open the following coincidence units (KO) for the accompanying time signals t_γ, thereby qualifying them as $t\gamma_1$ or $t\gamma_2$. This procedure is often called a slow (E_γ) - fast (t_γ) coincidence and is denoted by the letters SFC.

In order to measure the time difference $\Delta t = t\gamma_2 - t\gamma_1$, one uses $t\gamma_1$ and $t\gamma_2$ to start and stop a clock (TPC : time to pulse height converter), which in turn produces an analog pulse whose amplitude is proportional to the elapsed time interval Δt.

Eventually, the multichannel analyzer (MCA) receives the analog pulses and stores them in its memory according to their amplitudes. Finally, a histogram 'number of events I(t) versus time t' is created as shown in fig. 3.8.

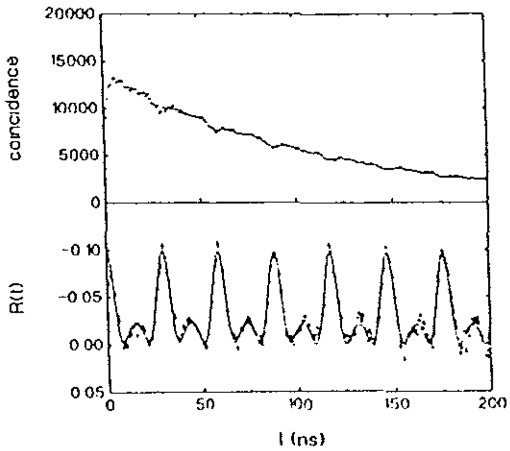

Fig. 3.8 Coincidence spectrum of the angular correlation $I(\theta,t)$ along with the extracted PAC time spectrum

An observation on the scheme in fig 3.7 sheds light on the possibilities of improving the set up so as to obtain higher detection efficiencies. The only requirement in this case will be analyzing each signal for $E\gamma_1$ and $E\gamma_2$ by elevating the status of each detector as a start and stop detector, so that two coincidence spectra are simultaneously recorded.

During the PAC experiments of this work a 4-detector set up was used in which each detector can act both as a start and stop detector. Apart from this, the aforementioned basic principles of the correlation set up are quite identical.

The 4 detectors used for the experimentation are arranged in such a way that each detector encloses an angle of 90^0 with its neighbour. In this manner, up to 12 coincidence spectra are measured at the same time from which the PAC time spectrum R(t) is obtained after the subtraction of the time independent background of accidental coincidences.

3.7 Probe atoms for PAC

The PAC technique is known for its special capacity in observing the $\gamma\gamma$ angular correlation. The technique meets this objective by using radioactive isotopes that emit as a cascade two γ-rays which should be easily distinguishable by their different energies $E\gamma_1$ and $E\gamma_2$.

The property of the intermediate nuclear state strongly determines whether a particular probe atom is suitable or not for a PAC experiment. The intermediate state should satisfy the following criteria [21].

(a) Its life time τ should lie between 10 and 1000ns for technical reasons. τ determines the time window during which the spin precession is observable.

(b) Its nuclear quadrupole moment should be large because it determines the magnitude of the spin precession frequency ω whose period $2\pi/\omega$ should be not much larger than the life time.

As regards to the excited state E_1 of the γ-γ cascade (fig.3.3) it has to be populated by a suitable parent isotope, which is often called the probe atom, instead of the daughter isotope, which provides the γ-γ cascade.

Moreover, the life time of the parent isotope is very important because it determines the time available not only for doping and treating the sample before conducting the PAC experiment but also the very performance of the PAC experiment itself.

The chemical nature of the parent isotope should also be considered as it determines where and how the probe atom is incorporated into the sample and whether there will be an interaction with the defects or not. Hence, the aforementioned criteria restrict considerably the list of candidates suitable as probe atoms.

3.8 PAC and Mössbauer Spectroscopy

It is interesting to compare PAC with other spectroscopic techniques which also measure hyperfine interactions.

The Mössbauer spectroscopy, like PAC, uses radioactive probe atoms and measures hyperfine interactions. It is found to be more than of academic interest to distinguish between their methods and limitations as well.

In PAC, the time window determines the largest and smallest observable frequency $\omega_0 = 2\pi/T_0$ with

$$2\tau_0 < T_0 \le 3\tau \tag{20}$$

where τ_0 is the time resolution of the detection system and τ is the life time the nuclear state.

In Mössbauer spectroscopy (MS), we have only the condition

$$\hbar\omega_0 > \Gamma \quad \text{or} \quad T_0 < h/\Gamma \approx \tau \tag{21}$$

where Γ is the natural line width of the Mössbauer resonance line. As it is readily seen in eq.(21) for MS a limit only for low frequences exists [19]. The lower limit is fixed by the width of the experimentally observed resonance line. In cases of greater line widths which could be attributed to absorber effects or unresolved lines, the low frequency limit will increase.

Hence, one point of difference is that PAC is more sensitive to low ω_0, whereas MS is more suited to detect high ω_0.

Moreover, MS is temperature dependent while PAC is not. Consequently it becomes more difficult to perform MS at higher temperatures. On the otherhand, temperature dependent dynamic effects can be studied by MS whereas this is not possible for PAC.Measurement of atomic jumps in diffusion can be done using MS.

In contrast to other spectroscopic techniques like NMR or ESR, PAC doesnot require an external applied field. Isomeric shifts can be detected by MS from the electric monopole term (Appendix A) On the other hand the precession frequency ω of nuclear spins can be detected using PAC from the quadrupolar interaction (Appendix A).

Hence, it can be seen that each experimental technique has a typical domain of problems to which it is strongly applied.

From the illustrative comparison between MS and PAC, it could be inferred that in many respects both techniques can be regarded as complementary hyperfine techniques.

CHAPTER IV

4. EXPERIMENTS ON THE BEHAVIOUR OF DIFFUSED LITHIUM ATOMS IN ^{111}In DOPED ZnSe

This chapter encompasses a series of experiments accomplished by diffusing Lithium into ^{111}In doped ZnSe.The generalized experimental objectives, procedural steps of sample preparation and motivations for diffusing Lithium are presented as they stood to be basic prerequisites of each experimental work which is fully discussed in light of the specific aims and achievements. In all experiments discussed here, the incorporation of ^{111}In and Lithium atoms is done by diffusion carried out under well defined temperature programmes. Sufficient information is extracted from the PAC time spectra of each sample subjected to typical experimental conditions.

A separate realization of Lithium induced effects was achieved using reference samples and employing special thermal treatments. The various dependences of the diffusion of Lithium on the matrix temperature, and the vapour pressure of Lithium are also investigated. Moreover, isothermal experiments were conducted to understand the time evolution of the $In_{Zn} - V_{Zn}$ fraction obtained from ZnSe samples treated at constant matrix and Lithium temperatures so as to investigate some aspects of the preceeding experiments.

4.1 OBJECTIVES OF THE EXPERIMENTS

The Lithium diffusion experiments on ZnSe samples doped with the radioactive dopant ^{111}In were accomplished for the following objectives:

1. To separately observe in particular Lithium induced effects from those effects generated by temperature, ^{111}In doping and stochiometric deviation via special thermal pretreatments and a systematic control of the vapour pressure of diffused Lithium atoms and the matrix temperature in a number of ways.

2. To investigate whether or not the observed Lithium induced effects on other II–VI compounds like CdS, ZnS and CdTe could as well be extended to the II–VI compound ZnSe.

3. To identify the causes of P-doping problems in ZnSe and to predict rectifying solutions for prospective work.

4.2 APPARATUS

Detectors: BaF_2 or NaI(Tl) scintillation crystal with photomultiplier XP 2020 philips

Amplifier: Delay line Amplifier Model 460 EG & G ORTEC

Single channel analyzer: SCA model 551 EG & G ORTEC

Constant fraction discriminator: CFD Model 2126 CANBERRA

Octal Discriminator: OD Model 623B LECROY

DUAL Mixer: DM Model AN308/NL EG & G ORTEC

Time to pulse height converter (TPC) Model 566 EG & G ORTEC

Level Adapter: (LA) Model 416A, EG & G ORTEC

A-D-changer and MCB : ADCAM Multichannel-Buffer Mode 918A

OTHERS

Quartz ampoulles, dosimeter, heating oven, thermocouples, Digital voltmeter, stop watch, a flame source, manometer, a Se chalcogenide, absorber, $InCl_3$ dissolved in HCl, tweezers, beambalance, and monitor

4.3 Sample Preparation Procedures

The aims of sample preparation procedures were the following:

A. To incorporate ^{111}In into the ZnSe samples by diffusion

B. To conduct the experiments successfully by subjecting the sample to well defined and measurable initial conditions

C. To foster the reproducibility and retracability of each of the conducted experiments

As the above goals imply, preparation of ZnSe samples and subjecting them to some physical pretreatments are crucial steps to be implemented by the experimentalist. In this connection, it is a well confirmed fact that the quality of physical information obtainable through an analysis of the respective PAC time spectra of the sample strongly depends upon the tidiness and orderliness of sample preparaion steps. The factors noted for their role in maximizing the safety during the radioactive steps are known to be called the 4A's in German since they all start with the letter A and they are stated below:

1. Time (to be minimized by an efficient procedure)
   Aufenthaltsdauer
2. Distance (to be regulated appropriately)
   Abstand
3. Activity (less activity to be maintained)
   Aktivität
4. Shielding (to be done to avoid the damage from some activity)
   Abschirmung

4.4 ACTIVATION

Activation is an experimental process with the help of which the II-VI compound semiconductor ZnSe is diffused with the radioactive probe atom ^{111}In before it is employed as a sample to be investigated using the powerful PAC technique. Indeed, all thermal pretreatments in the process are categorized under activation. In literal terms activation could mean adding some radioactivity into the ZnSe samples.

4.5 ACTIVATION PROCEDURE

Slices of oriented ZnSe crystals were cut and their dimensions were measured. Sample shapes and other particular features were noticed as well. Moreover, the important equipments like quartz ampoulle, pair of tweezers, absorber and other apparatus listed above were arranged before-hand after which a regulated checking of left over activity was accomplished. Afterwards the temperature of the heating oven was adjusted to the value 1070K for the subsequent thermal treatment of the sample which was etched in a saturated HCl solution to remove some impurities. The heating oven was given equilibrating time to adjust itself to the above mentioned temperature. In the meantime, a short-sized quartz ampoulle (length=16cm) was made ready inside which a small piece of quartz was inserted afterwards.

To clean the ampoulle and the quartz piece from some volatile impurities, the H_2-O_2 flame source (burner) was used. In this step, the respective oxygen and hydrogen taps were opened and adjusted until a flame having the right size, strength (intensity) and color has resulted. Then, the quartz ampoulle was rotated around its axis in the flame, a passage being made after a white circular ring is formed. The heating helped to clean the inside part of the ampoulle from some impurities which may vapor out during such a procedure. The cleaned quartz piece was removed from the quartz ampoulle so as to deliver the radioactive solution ($^{111}InCl_3$:HCl) onto it. To absorb the radioactive solution, the volume level was adjusted by setting the right sequence of digits on the wall of the absorber. Desired values of volume in microlitres (1–3$\mu\ell$) were adjusted and a cone-shaped plastic was plugged at the absorber's tip for absorption. After the solution was absorbed, it was dropped onto the quartz piece. From this solution about 10^{11} In atoms were offered. In order to dry the solution, the quartz piece was kept under a switched on lamp for about 5 minutes. Afterwards, the quartz piece was inserted into the quartz ampoulle containing the sample, and the ampoulle was kept at a lead shielded corner to avoid the damage from the radioactivity.

To accelerate the incorporation of Indium into the II-VI compound ZnSe sample, few milligrammes of the chalcogen Selenium (Se) was added into the quartz ampoulle behind a lead shield.

The added selenium used to offer the required chalcogen over pressure (about 86 mbar) and it used to create stochiometric deviations in the sample by creating Zinc vacancies in the metal sublattice of the ZnSe crystal. It was a remarkable fact that, in general, the chalcogen amount to be added depends upon the particular II-VI system one is dealing with and on the type of chalcogen as well. In my case, about 0.6 mg of Se was added while activating the ZnSe samples.

As Selenium is a fine and slippery powder, it was a successful method to melt and collect it in a solidified form as this helped in measuring its mass in a controllable way.

In the next step, the quartz ampoulle was evacuated up to a vacuum of 10^{-5}bar. This evacuation process helped to distinctly realize the over pressure of the added chalcogen (Se) from the pressure of the air preexisting in the quartz ampoulle. After a regulated rotation of the ampoulle at one fixed point, the glass was getting thinner and thinner at the heated region and eventually it was detached from the other portion of the glass.

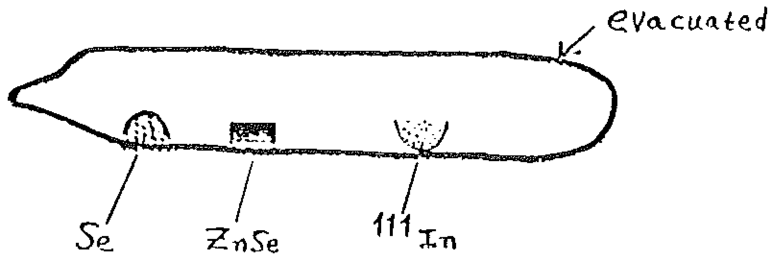

Fig. 4.1 A schematic diagram of the Sealed quartz ampoulle inside which the ZnSe sample, the ^{111}In: HCl solution and the molten Selenium are placed side by side

The quartz ampoulle's part containing the sample and the added components was then sealed by the flame. Fig 4.1 shows the schematic diagram of the sealed quartz ampoulle.

After the sealed portion of the ampoulle was cooled, the sample inside and the quartz piece were localized to the unheated edge of the quartz ampoulle. Eventually, the sealed quartz ampoulle was inserted into the preheated oven at the site of the right thermocouple. In the oven, the sample was kept overnight for 15 hours at the equilibrated temperature of 1070 K.

Following the completion of the long heating process, the sample was quenched (cooled). The type of quenching depends upon the value of the starting $In_{Zn} - V_{Zn}$ paired fraction that is aimed to be achieved. The faster the type of quenching, the smaller will be the $In_{Zn} - V_{Zn}$ fraction due to the freezing of the vacancies, V_{Zn}. After the quenching process was done, the PAC time spectrum measurement of the "as diffused" sample was taken. The term "as diffused" refers to a sample which is freshly activated. Indeed, the above mentioned procedure is common to all PAC experiments.

4.6 Results of ^{111}In Diffusion

The diffusion of ^{111}In into ZnSe was successfully accomplished with a transition rate of 85%, that is 85% of the offered Indium atoms on the quartz piece were transferred to the sample. This was obtained by comparing the activity of the "as diffused" sample with the activity offered on the quartz piece. The diffused Indium atoms penetrated to a depth of about 5μm as etching experiements showed, and that yielded a local concentration of In atoms to be about $10^{15}/cm^3$ for a characteritic sample dimension.

As it is depicted in the PAC time spectrum of the "as diffused" sample in fig. 4.2 most of the ^{111}In probe atoms sat on regular lattice sites and evidently the goal of incorporating ^{111}In atoms on the Zinc site was achieved. This result is in acoordance with the observation that In acts as a donor in II-VI semiconductors[23]. The coupling constant ν_Q was found to be 72 MHz, and the asymmetry parameter η = 0.05. These values characterize the metal vacancy, V_{Zn} .Moreover, the largest component of the EFG is observed to be oriented along the <111> lattice direction in ZnSe.

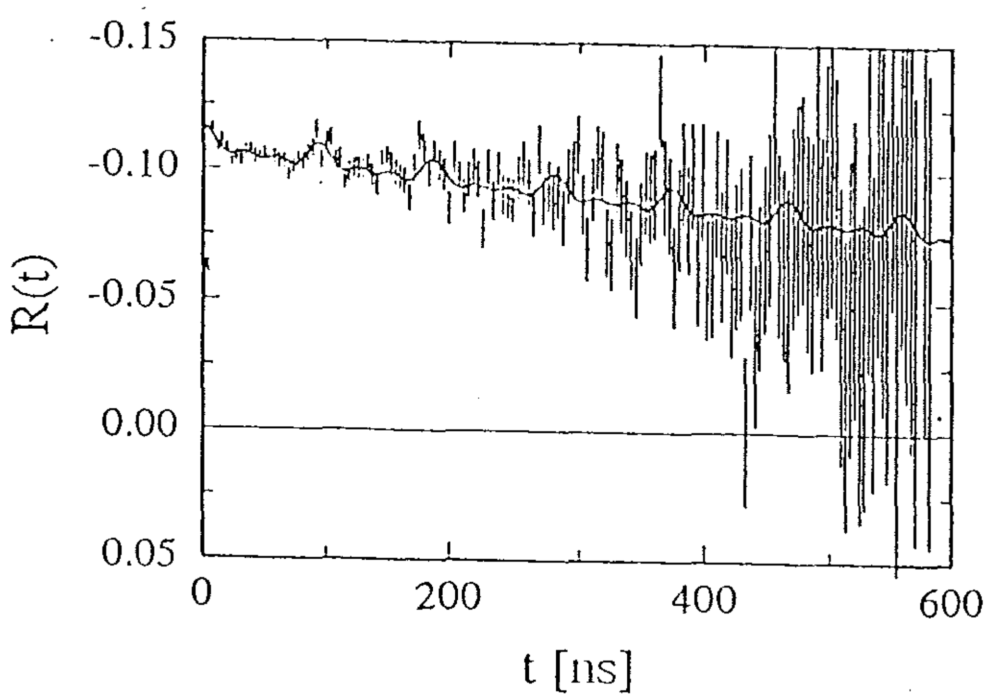

Fig. 4.2 Results of ^{111}In diffusion into ZnSe. In_{Zn} is achieved

4.7 Motivation for diffusing Lithium atoms into ZnSe

The central source of motivation for choosing Lithium atoms as possible dopants in ^{111}In doped ZnSe samples was the fact that ZnSe can easily be doped n-type, whereas it is difficult, if not impossible to make it p-type.

The difficulty in p-doping ZnSe is attributed to the strong interaction of P-dopants with intrinsic defects leading to the self compensation phenomena. However, if ZnSe can be made p-type, it becomes an attractive candidate for the blue green laser diode and this has been a strong motive for researchers in this area.

If successful, Lithium atoms introduced on the Zinc site will serve the desired task of p-doping ZnSe. As to inquire and investigate the possibilities and challenges of this Lithium-doping, a series of Lithium diffusion experiments were conducted to investigate the incorporation of Lithium into ZnSe in an atomic scale. As donor-acceptor coulombic interactions were observed from PAC experiments conducted on Silicon, Germanium and several other III-V semiconductors[24] it was the main motivation for diffusing Lithium into ZnSe so as to prove if there was also donor (In_{Zn}) – acceptor (Li_{Zn}) interaction observable by PAC from the specific finger print of the defect, Li_{Zn}.

Fig. 4.3 shows the atomistic picture of a unit cell of the ZnSe crystal doped with ^{111}In. From the figure it is clear that, if successful Lithium atoms taking the substitutional Zn site guarantee the p-doping in ZnSe. If this is possible, the PAC technique should be able to observe it from the coulombic donor-acceptor interactions. Some observations were made from the PAC spectra of Lithium diffused ZnSe samples in the past. Whether new Lithium specific finger print is observed or not is answered in the subsequent section by displaying the observed PAC spectra.

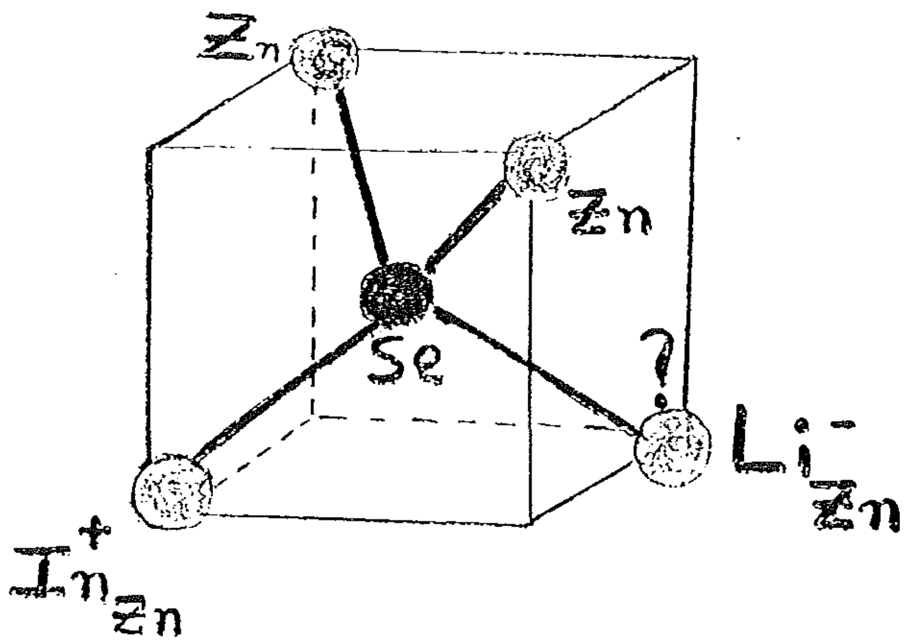

Fig. 4.3 A unit cell of the ZnSe crystal. Donor—acceptor, i.e. (In_{Zn} – Li_{Zn}) interactions are expected to be observed by PAC

4.8 Observations

As a preliminary accomplishment to study the effects of diffused Lithium atoms into ZnSe, it was necessary to start with the observations of such effects from published results[23].

Such a preobservation laid the basis to devise a consistent strategy for the investigation of Lithium induced effects using the PAC technique. The observed effects are represented in fig. 4.4. Shown in this figure are the R(t) spectra and their corresponding Fourier transforms of two ^{111}In doped ZnSe samples: top (without Lithium), bottom (with Lithium) where other thermal treatments were the same in both samples.

From a comparative observation of the two graphs it is noticed that:

(1) No Lithium specific finger print (i.e. Lithium taking a substitutional Zn site or Li_{Zn}) was observed as there was no strange pattern in the PAC spectra of the Lithium diffused sample when compared to the reference sample (sample without Lithium).

(2) The PAC spectra of the Lithium diffused sample showed a pronounced modulation of the R(t) spectra and the enlargement of the amplitudes of the frequencies in the Fourier transforms. Both effects stand on the same footing and they confirm the formation of a maximized In_{Zn} - V_{Zn} paired fraction following Lithium's diffusion. Indeed, in both cases, ν_Q=72MHz and η = 0.05 were obtained still characterizing the same defect (V_{Zn})

Hence, from the pronounced increase of the In_{Zn} - V_{Zn} pair fraction in the Lithium diffused sample it is concluded that Lithium induces vacancies (V_{Zn}) and subsequently its incorporation is visible as an enhancement of the In_{Zn} - V_{Zn} paired fraction. Previous measurements [23] also confirm the observation of the same effects in other Li diffused II-VI compounds like CdS, ZnS and CdTe. In this project, a series of experiments were conducted to indirectly investigate the incorporation of Lithium (the "cause") from the values of the In_{Zn} - V_{Zn} pair fraction (the "effect") by employing special thermal treatments which led to new interpretation of the results.

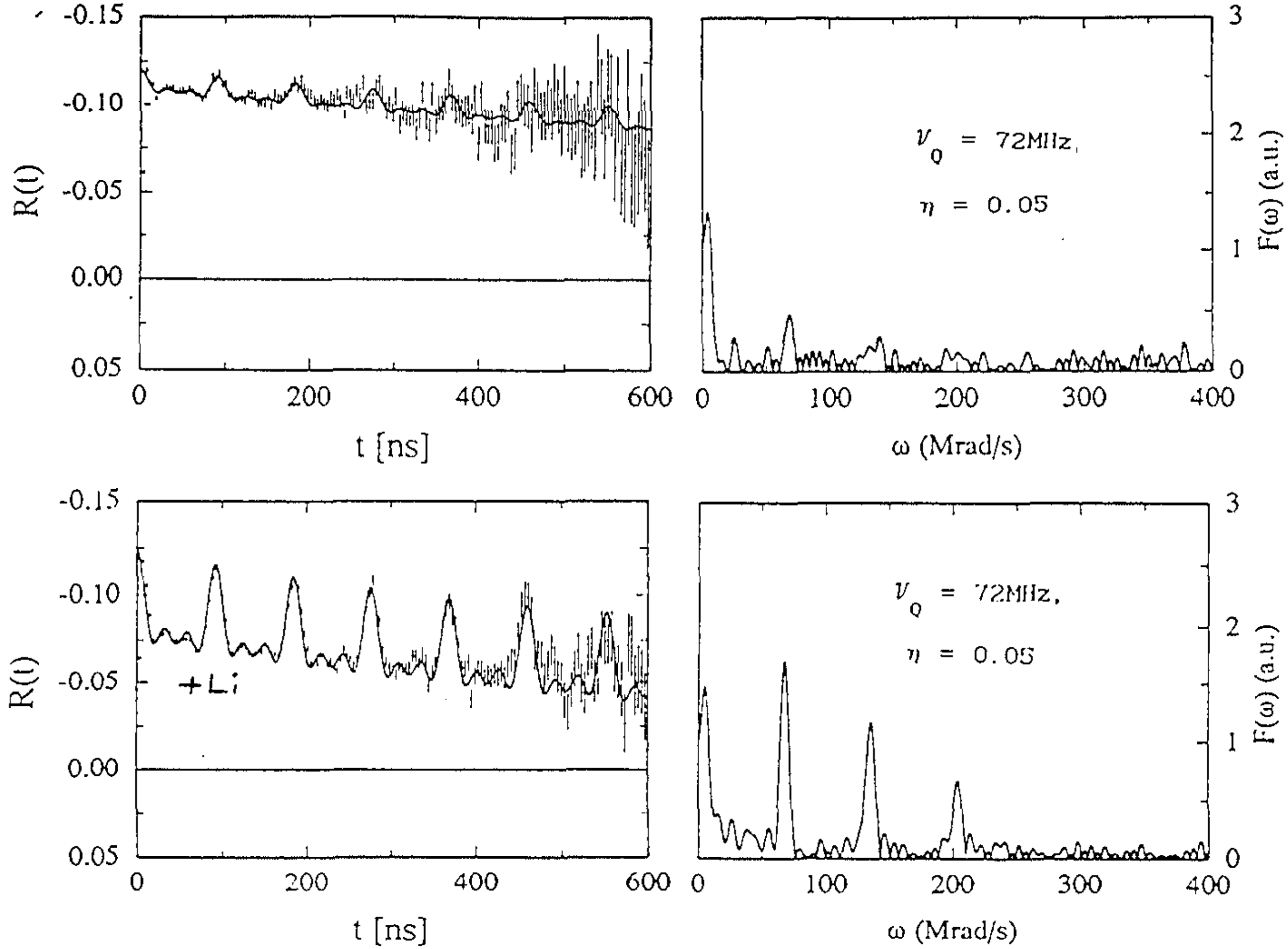

Fig. 4.4 (Top): The R(t) spectra and its Fourier transform $F(\omega)$ of a ZnSe sample doped only with ^{111}In.

(Bottom): R(t) and the corresponding $F(\omega)$ for the ZnSe sample doped with both ^{111}In and Lithium

4.9 POST TREATMENT

Post treatment is a subsequent physical treatment of the sample after a first hand ("as diffused") PAC time spectra measurement is taken. It can be regarded as a transitional treatment of the sample via pre subjecting it to controllable factors for the forth coming experimental goals. As how to post treat the sample depends upon the particular objectives the experimentalist wants to realize in the subsequent experiments to be done on the same sample. This treatment offers new physical conditions to the sample. Temperature is one such condition and it affects the vacancy distribution in the sample. The process also helps to separately identify responsible factors for changes in the numbers of $In_{Zn} - V_{Zn}$ pairs in the planned experiments.

Specifically, post treatment helps to separate between metal vacancies created by self compensation due to ^{111}In doping or chalcogen over pressure induced vacancies by stoichiometric deviations from those generated by self compensation due to a dopant like Lithium.

4.10 Reducing intrinsic defects

Before diffusing Lithium into ZnSe samples, they were heated to a temperature of 900K for 30min. The principal goal of this post treatment was to reduce intrinsic defects existing in ZnSe by making use of thermal dissociational effects of the $In_{Zn} - V_{Zn}$ pairs as it is well established from the dissociation curve shown in fig. 4.5.

It must be attentively noticed that such a post treatment enables the experimentalist not only to set a well defined initial condition for the Lithium diffusion but also to realize the reduction of intrinsic defects thereby standing at a safer position to separately observe Lithium induced effects via excluding some possible superimpositions of similar effects generated by other factors.

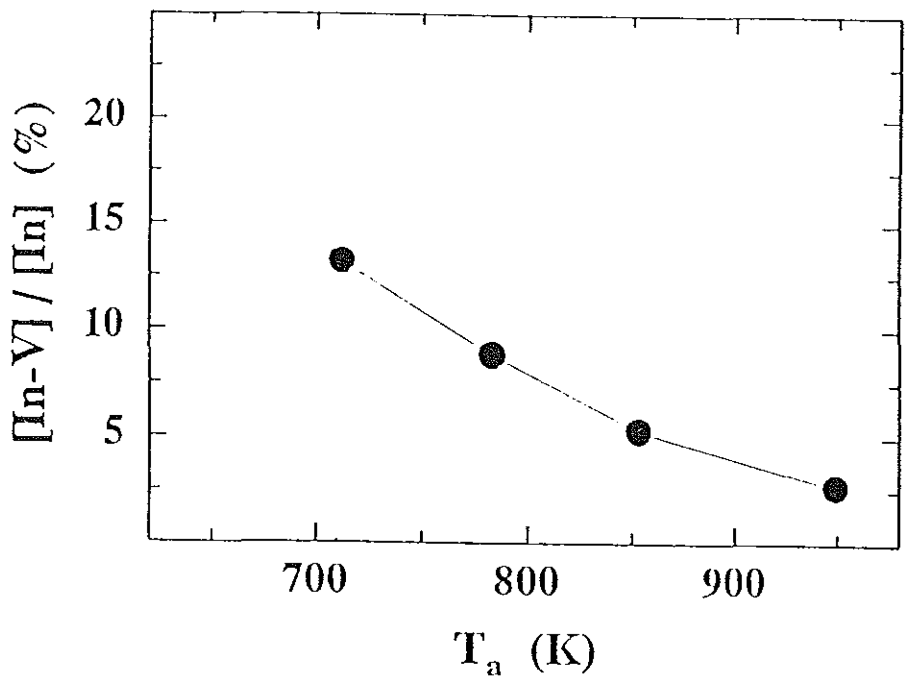

Fig. 4.5 Annealing Samples at 900K/30min reduces intrinsic defects [23].

4.11 Diffusion of Lithium into ZnSe

The metallic Lithium was cut in a small piece and its surface was smoothly scratched to clean some clinging impurities. Moreover, the Lithium piece was soaked in a diluted HCl acid to remove some oxides from it.

The metallic Lithium and the activated ZnSe samples were arranged inside a sealed and evacuated quartz ampoulle as it is depicted in the schematic diagram in Fig. 4.6.

Since Lithium in the vapour phase must diffuse into the ZnSe sample, the diffusion process was carried out by preparing well defined diffusion conditions like diffusion temperature and diffusion duration. The effect of the diffusion was studied for restricted temperature ranges. In these experiments, special attention was devoted to studying the effects of the vapour pressure of Lithium (P_{Li}) which is controlled by the temperature of Lithium and the effects of the matrix temperature (i.e. the temperature of ZnSe) in governing the solubility of Lithium atoms into ZnSe.

Hence, it was planned to carry out the diffusion experiments by monitoring the two temperatures: the temperature of ZnSe and the temperature of lithium independently. To realize this indpendent temperature control, a 2-zone oven whose schematic diagram is showed in fig.4.7 was employed. The oven posseses two heating regions: the main heating zone and the additional heating zone. The adjoining graph below it shows the temperature distribution at the various positions in the oven. In this connection, the experimentally accessible temperature range is shown to be the region bounded by the trapezium drawn in fig. 4.8.

It is a remarkable fact that $T_{ZnSe} > T_{Li}$ within the bounded region (explained in fig.4.8)except the technical restriction that limits T_{ZnSe} not to exceed T_{Li} by more than 350K. The region for which $T_{Li} > T_{ZnSe}$ is a forbidden region since it results in the undesired over condensation of Lithium onto ZnSe.

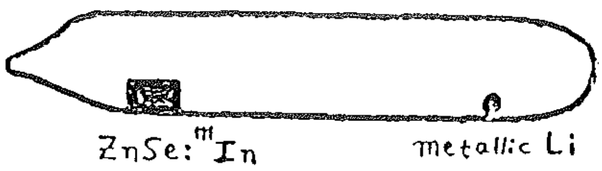

Fig. 4.6 Arrangement of ^{111}In doped ZnSe and the metallic Li in a sealed quartz ampoulle

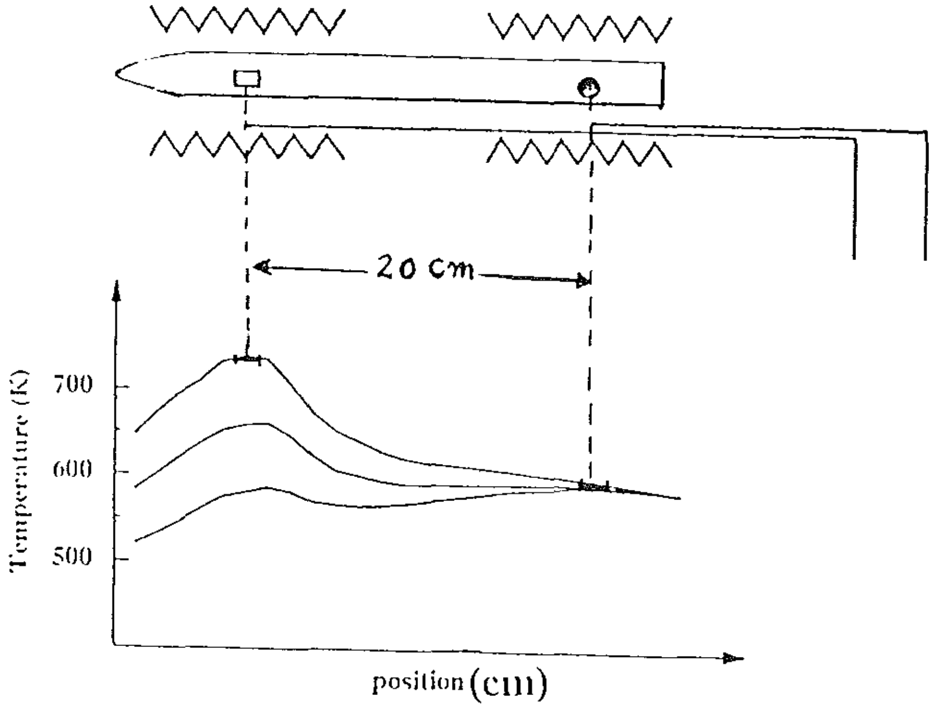

Fig. 4.7 The two zone oven with the graph below it showing the temperature distribution in it

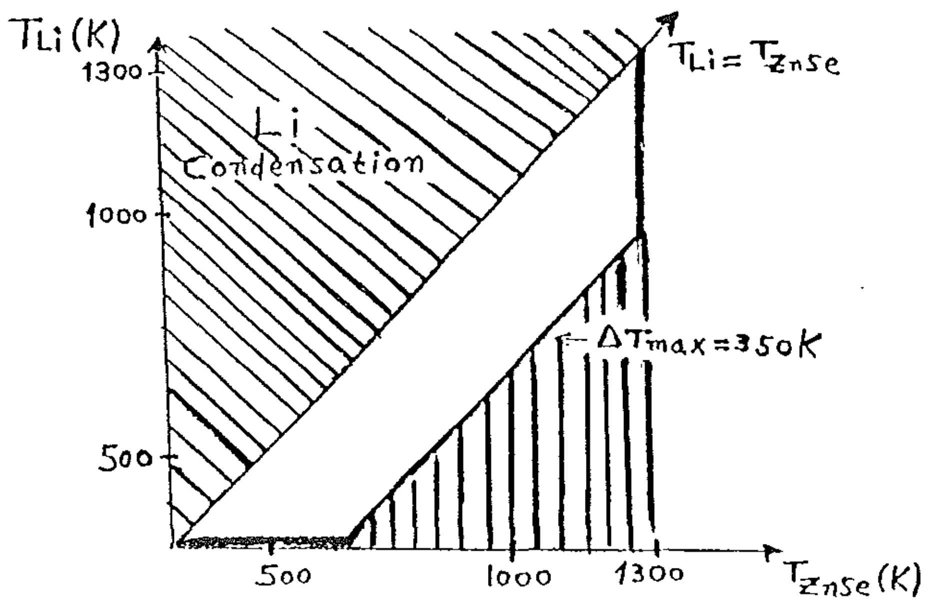

Fig. 4.8 The accessible temperatures lie in the region bounded by the trapezium in which $T_{ZnSe} > T_{Li}$. This was done to avoid the over condensation of Lithium onto ZnSe. The temperature region defines favourable diffusion conditions .For technical reasons, $T_{ZnSe} - T_{Li} \leq 350K$ The origin corresponds to a room temperature value.

4.11.a Preparation for PAC measurements

Preceeding to every PAC measurement and after each Lithium diffusion, the ZnSe samples were heated to 550K/for 30 min. As is depicted in the "formation-dissociation" curve shown in Fig. 4.9 this thermal treatment effects mobilization of isolated vacancies created by a pretreatment like heating or doping. Subsequently, most of the Zinc vacancies will be trapped by the Indium atoms, yielding a high value of the $In_{Zn} - V_{Zn}$ fraction that delivers a vital information on the absolute number of vacancies created by a pretreatment.

4.11.b The investigated temperature range

The triangle drawn in fig 4.10 shows the investigated temperatures for the diffusion experiments. These temperatures were adjusted in the two zone oven. The diffusion time was 30 min.

The three diffusion conditions were:

1. $T_{Li} = T_{ZnSe}$
2. $T_{Li} = \text{const.}$
3. $T_{ZnSe} = \text{const.}$

4.12. EXPERIMENTAL RESULTS AND DISCUSSION

Experiment 1: Diffusion of Lithium into ZnSe with the condition $T_{Li} = T_{ZnSe}$

This experiment was conducted on two ZnSe samples: a lithium diffused sample and a reference sample. The ZnSe single crystals were first diffused inside an evacuated quartz ampoulle with the radioactive ^{111}In atoms (1070K/15h, 86 mbar Se overpressure). The sample was cooled by a vacuum quench via a fast immersion of the closed quartz ampoulle into water. Both samples were subjected to a post treatment of 900K/30min to reduce intrinsic V_{Zn} defects. The diffusion of Lithium was accomplished after this step and both samples were heated at 550K/30min to mobilize the created vacancies after each Lithiumdiffusion andthecorrespondingthermal treatments.

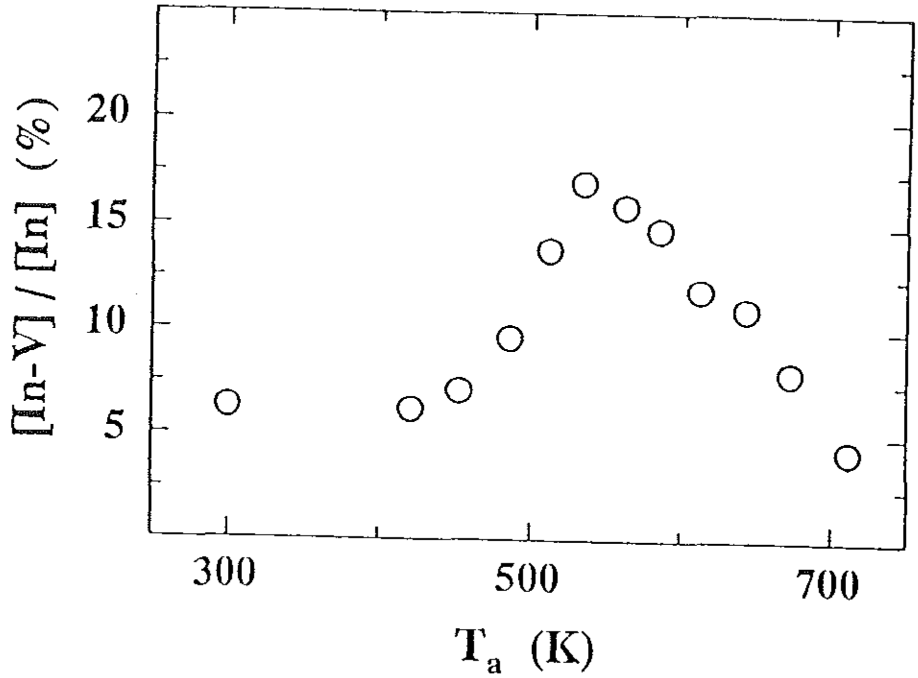

Fig. 4.9 Annealing samples at 550K/30min mobilizes vacancies and yields large values for [In-V]/[In] [23]

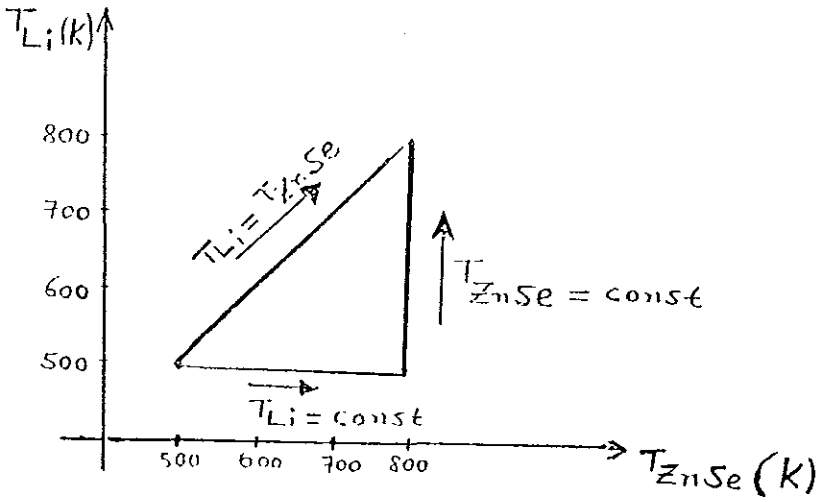

Fig. 4.10 The investigated temperature range which lies in the accessible temperature region of Fig. 4.8.

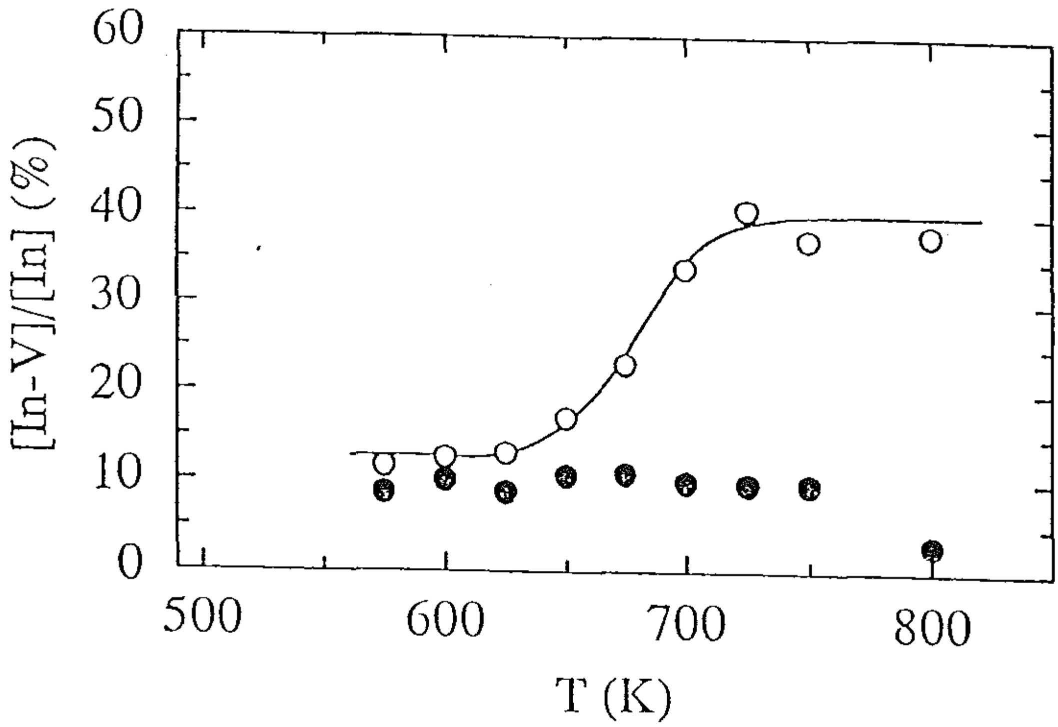

Fig. 4.11 The result of exp. 1.The result of exp.1.with the condition $T_{ZnSe} = T_{Li}$ where the diffusion time, t_D = 30 min. The open circle data points (O) represent the Lithium diffused sample where as the reference sample is represented by the closed circle data points (●).

This is the back bone result of our experiments.

Notice that the pronounced increase in the fraction in the Lithium diffused sample is caused by Lithium (Li induces Zinc Vacancies, V_{Zn}^{--})

The graph shown in fig. 4.11 shows the result of this experiment. As it is seen in this graph, the Lithium diffused sample is represented by the open circle data points where as the closed circle data points represent the reference sample. The starting temperature was 575K and a temperature interval of 25K was selected to observe the effect of Lithium diffusion in a smooth manner. The reference sample (closed circles) underwent the same thermal treatment without the presence of Lithium.

It is noticeable that the In_{Zn} – V_{Zn} fraction in the Lithium diffused and reference sample were comparable up to the temperatures 575K, 600K and 625K.

However, in the Lithium diffused sample (open circles) there is a remarkable increase in the fractions starting from T = 650K until saturation is reached at 725K The highest value for the fraction was 41% and it was observed at T = 725K. Moreover, it is remarkable that the treatment of the sample with Lithium at only 725K produces four times as much In_{Zn} – V_{Zn} pairs compared to the reference sample treated at the same temperature. Since the fractional increases are evidently absent in the reference sample, the presence of Lithium is the cause for the accelerated In_{Zn} – V_{Zn} fraction observed in the Lithium diffused sample.

Furthermore, it should be noted that thermally created V_{Zn} defects can not be the causes for the strong increase of the paired fraction in the Lithium diffused sample as this was not observed in the reference sample undergoing the same thermal treatment except the absence of Lithium. Since the reference sample showed no increase in the In_{Zn} – V_{Zn} fraction, no isolated V_{Zn}defects were left in it and this fact confirms the success of the special thermal post treatment at 900K/30min. in reducing the intrinsic VZn defects.

The observed decrease in the $In_{Zn} - V_{Zn}$ paired fraction for the higher temperatures at T = 750K and T = 800K can be explained by a thermal dissociation of the preexisting $In_{Zn} - V_{Zn}$ pairs. This dissociational effect is more serious in the reference sample than in the Lithium diffused sample as Lithium induced vacancies replace the site of the thermally migrating vacancies in the latter.

4.12.a Discussion

The experimental graph depicted in fig. 4.11 is the "backbone" result of the diffusion experiments. For the investigated temperature range 575K ≤ T ≤ 800K no donor – acceptor pairing of the type In_{Zn}-Li_{Zn} is observed by PAC which implies that Li_{Zn} states are not measurably populated. As is observed, when Lithium is diffused into ^{111}In doped ZnSe the formation of the $In_{Zn} - V_{Zn}$ pairs is enhanced and from the special thermal treatments, it can be concluded that the deep increase in the $In_{Zn} - V_{Zn}$ pairs must be caused by Lithium induced vacancies. Moreover, this effect is quite remarkable and may shed new light on the mechanism that is responsible for p-doping of ZnSe.

A reaction governing the incorporation of Lithium in a II–VI crystal can be stated as:

$$Li_M^- \rightleftarrows Li_i^+ + V_M^{--}$$

where the subscripts M and i respectively denote the metallic lattice site and an interstitial site.

For ZnSe, the above reaction can be written as

$$Li_{Zn}^- \rightleftarrows Li_i^+ + V_{Zn}^{--}$$

Indeed, this reaction is strongly shifted to the right hand side for the investigated temperatures in 650K ≤ T ≤ 800K. The complex defect at the right hand side of the above reaction, formed by the interstitial Li_i and the Zinc vacancy, V_{Zn} can still act as a single acceptor and, therefore, can produce p-conductivity in ZnSe [23].

Hence, it can be inferred that Lithium induces new vacancies, V_{Zn} which consequently leads to a pronounced formation of the In_{Zn} – V_{Zn} pairing. For the Lithium in ZnSe, Sasaki and Oguchi [24] arrived at the conclusion that the acceptor Li_{Zn} is unstable against disintegration into a vacancy V_{Zn} and interstitial Li_i. Moreover, PAC experiments done on CdS, ZnS and CdTe show a common behaviour of the Lithium atoms despite the variations of these II–VI compounds in the band gap energies and bonding mechanisms[23]. Indeed, the same intrinsic defect, the metallic vacancy V_{Zn} determinies the state of In atoms to be a donor state (In_{Zn}) and minimizes acceptor states of Lithium (Li_{Zn}). This could possibly mean that the thermodynamic stability of the Lithium induced acceptor Zinc vacancies (V_{Zn}) requires the existence of Lithium atoms in interstitial donor states (Li_i) for electrical neutrality.

4.12.b Motivation for new experiments

Since the first experiment was accomplished with $T_{ZnSe} = T_{Li}$, obviously the effects of the sample's temperature and the temperature of Lithium are superimposed in causing the pronounced increase in the $In_{Zn} - V_{Zn}$ pairs.

However, the extent of their individual effect in governing the incorporation of Lithium was not observed. Hence new experiments were designed by varying T_{Li} where the matrix temperature, T_{ZnSe} is kept constant. Similar experiments were also conducted by varying T_{ZnSe} and fixing T_{Li} at a constant value. The results of these experiments illuminated the independent effects of the vapour pressure of Lithium (P_{Li}) and the matrix temperature (T_{ZnSe}) in governing the incorporation of Lithium atoms into ZnSe crystal.

4.12.c Experiment 2

Independent Variation of P_{Li} by fixing T_{ZnSe}

The aim of this experiment was to investigate the effect of increasing the vapour pressure of Lithium in governing the diffusion of Lithium atoms into ZnSe sample kept at 700K. The motive for choosing T_{ZnSe} =

700K (look the result of exp.1 in fig. 4.11) was the observed fact that in the neighbourhood of this temperature, the $In_{Zn} - V_{Zn}$ fraction was progressively increasing without yet reaching the saturation value. Lithium was diffused starting from T_{Li} = 450K up to T_{Li} = 525K in 25K steps. The diffusion time was t_D = 2hrs. Conducting the diffusion process beginning from a small T_{Li} and on small temperature increments guaranteed an observation of the smooth evolution of the P_{Li}. The result of this experiment is shown in the graph in fig. 4.12.

We conclude from this graph that the region 400K – 500K is a dynamic range, i.e. a range in which a steep increasing in the $In_{Zn} - V_{Zn}$ pairing is noticed. Nevertheless, comparison of the 4^{th} data point with respect to the 3^{rd} data point on the same graph shows a saturation tendency for the effect of the vapour pressure of Li on the $In_{Zn} - V_{Zn}$ fraction. (Look the result of experiment 4)

4.12.d <u>Experiment 3</u>

<u>Independent Variation of Sample's temperature by fixing Lithium's temperature</u>

This experiment was designed to investigate the effect of varying the sample temperature on governing the solubility of Lithium atoms at a fixed temperature T_{Li} = 500K into ZnSe sample whose temperature was varied over 75K steps from 500K to 800K.

The result of this experiment is plotted in fig 4.13. As it is noticeable from this graph, the temperature region 600K $\le T_{ZnSe} \le$ 800K is seen to be the dynamic range since the $In_{Zn} - V_{Zn}$ fraction value showed a corresponding increase.

However, the fractional increase is observed to be a very slow one compared to the result of experiment 2.

Hence, it can be concluded that the law governing the incorporation of Lithium atoms in ZnSe has different dependences on P_{Li} and T_{ZnSe}.

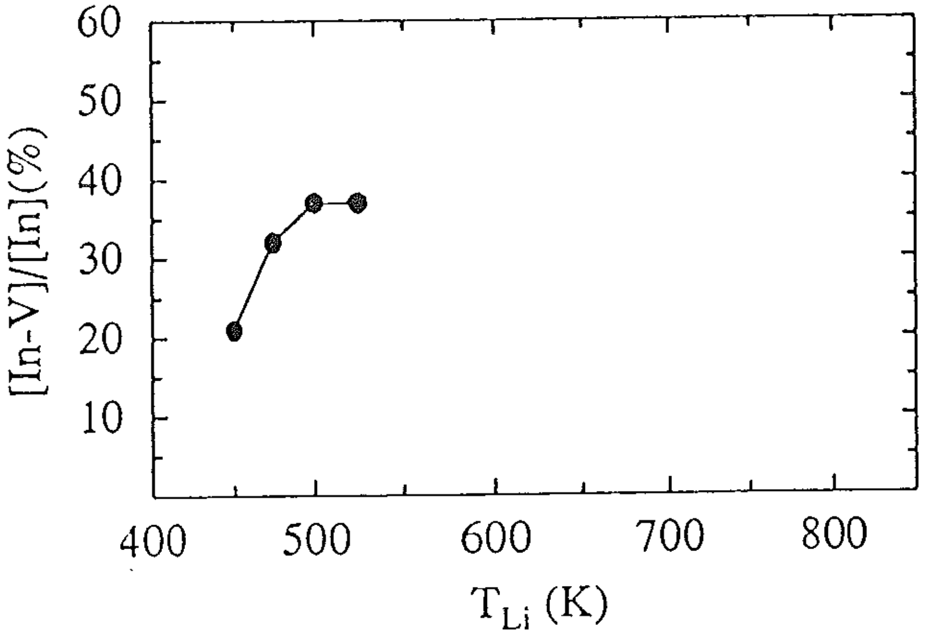

Fig. 4.12 Result of exp.2

The steep increase in the In_{Zn}- V_{Zn} fraction is caused by the vapour pressure of Li. Here T_{ZnSe} was fixed at 700 K Observe that since t_D = 2 hrs, f = 40% is already reached at T_{Li} = 500 K (compare it with exp.1.)

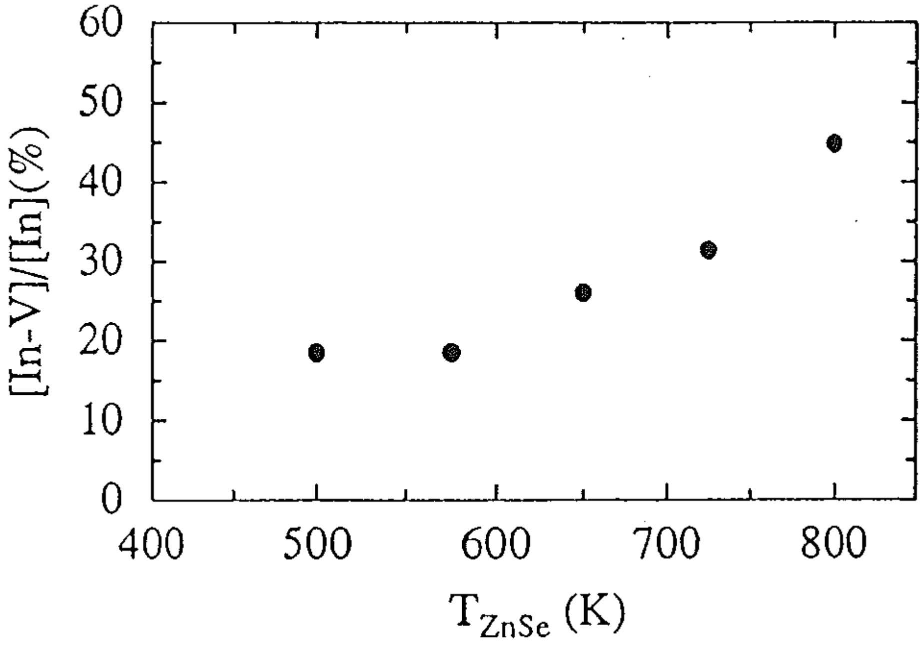

Fig. 4.13 Result of exp. 3

A slow increase in the In_{Zn} – V_{Zn} fraction is observed when T_{ZnSe} is varied. T_{Li} ≡ 800K

In this connection, the pronounced increase of the $In_{Zn} - V_{Zn}$ fraction observed in the first experiment under the condition $T_{ZnSe} = T_{Li}$ in the Lithium diffused sample seems to be caused more dominantly by the increased vapour pressure of Lithium in the range 650K ≤ T ≤ 725K.

4.12.e Experiment 4

Variation of P_{Li} over a wide temperature range

After the steep increase of the $In_{Zn} - V_{Zn}$ paired fraction in experiment 2, there seemed to be a saturation tendency for the effect of P_{Li}. Subsequently, this experiment was conducted to observe experimentally whether the predicted saturation tencency was reached or not. The sample employed in experiment 3 was reused in this experiment by fixing T_{ZnSe} at 800K and varying the temperature of Lithium over a wide range of temperature, i.e. 500K ≤ T_{Li} ≤ 800K. The strategy in choosing this wide temperature range was to investigate the effects of higher vapour pressure of Lithium on the fraction and carrying out the diffusion of Lithium over 75K temperature gaps was vital to observe the effect of P_{Li} in a smooth manner.

The graph in fig. 4.13 shows the result of this experiment. It is evident from this graph that there was no further increase in the $In_{Zn} - V_{Zn}$ pair fraction irrespective of the increases in P_{Li}.

Hence, it can be firmly concluded that the saturation value for the $In_{Zn} - V_{Zn}$ pair fractions was reached and higher values of P_{Li} showed no further effect on this fraction.

4.12.f Motivation for isothermal experiments

In the above mentioned four experiments, the effects of the sample temperature (T_{ZnSe}) and the Lithium temperature (T_{Li}) on the diffusion of Lithium atoms into ZnSe was investigated for a fixed diffusion duration, consequently the effect of varying the diffusion time was not considered.

Hence, new Lithium isothermal experiments were planned to investigate the time dependence of Lithium diffusion.

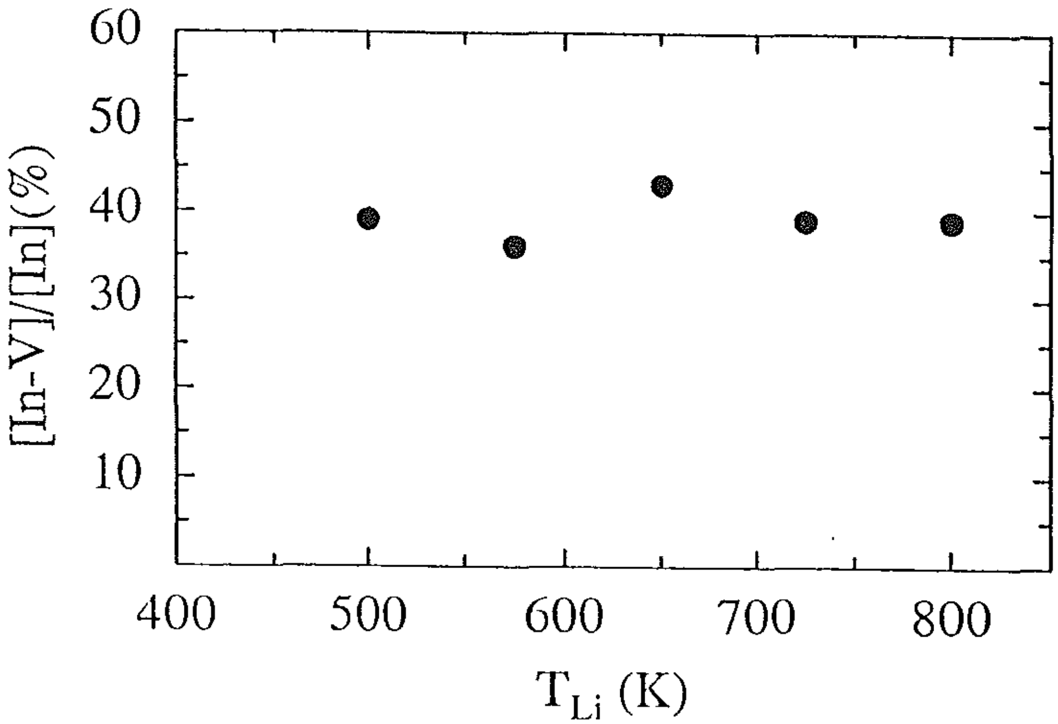

Fig. 4.14 Result of exp.4

Saturation for the value of $In_{Zn} - V_{Zn}$ is reached by varying P_{Li} over a wide range. $T_{ZnSe} = 800K$

The sample in exp.3 was reused here.

4.12.g Experiment 5

Investigation of the time dependence of Lithium Diffusion

This experiment was conducted on two different ZnSe samples in both of which the temperature of Lithium was fixed at T_{Li} = 500K where as the sample temperatures are kept at T_{ZnSe} = 650K and T_{ZnSe} = 725K respectively.

The motive for choosing the temperatures 650K and 725K for T_{ZnSe} is contained in the result of exp. 3 (look fig. 4.13). As it is evident there, the temperatures 650K and 725K belong to the dynamic range. Also, since the diffusion time in exp.3 was 30 min, the increasing tendency at the graph was interesting to investigate the effect of elongating the diffusion time on the incorporation of Lithium atoms into ZnSe.

The result of this experiment is graphically presented in fig. 4.15. At the top of this figure, the result of the isothermal experiment at T_{Li} = 500K and T_{ZnSe}= 650K is presented. The graph below it displays the result of the isothermal experiment at T_{Li} = 500K and T_{ZnSe} = 725K.

Notice that the two samples have comparable "as diffused" values. It is also observed from both graphs that a longer diffusion time of Lithium yields a pronounced increase in the fraction f. Hence the incorporation of Lithium atoms over a widened diffusion duration is ensured.

It should be attentively noticed that the sample with higher matrix temperature (T_{ZnSe} = 725K) showed a larger saturation fractional value (36%) when compared to the value obtained from the sample with a lower matrix temperature (T_{ZnSe} = 650K), which was only 27% (look fig. 4.16 for comparison).

A comparison of the fractional values observed at T_{ZnSe} = 650K and T_{ZnSe} = 725K (i.e. the 3rd and 4th data points of exp. 3) (fig.4.13) with the above saturation values obtained from the isothermal experiments confirms that there is no considerable difference between a diffusion duration of 30 min and a longer time in the observed fractions. Thus it can be concluded that a 30 min. diffusion duration is sufficient to observe the influence of T_{ZnSe} on the fractions.

Moreover, it is worthwhile to notice in fig 4.15 that in both samples the fractions converge to the equlibrium value after a comparable time. In other words, the time constant τ of the two diffusion processes is observed to be independent of the two matrix temperatures (T_{ZnSe} = 650K and T_{ZnSe}=725K). τ = 15 min. in both cases. Further investigations are necessary to extract the dependence of τ upon T_{Li} and other matrix temperatures as well.

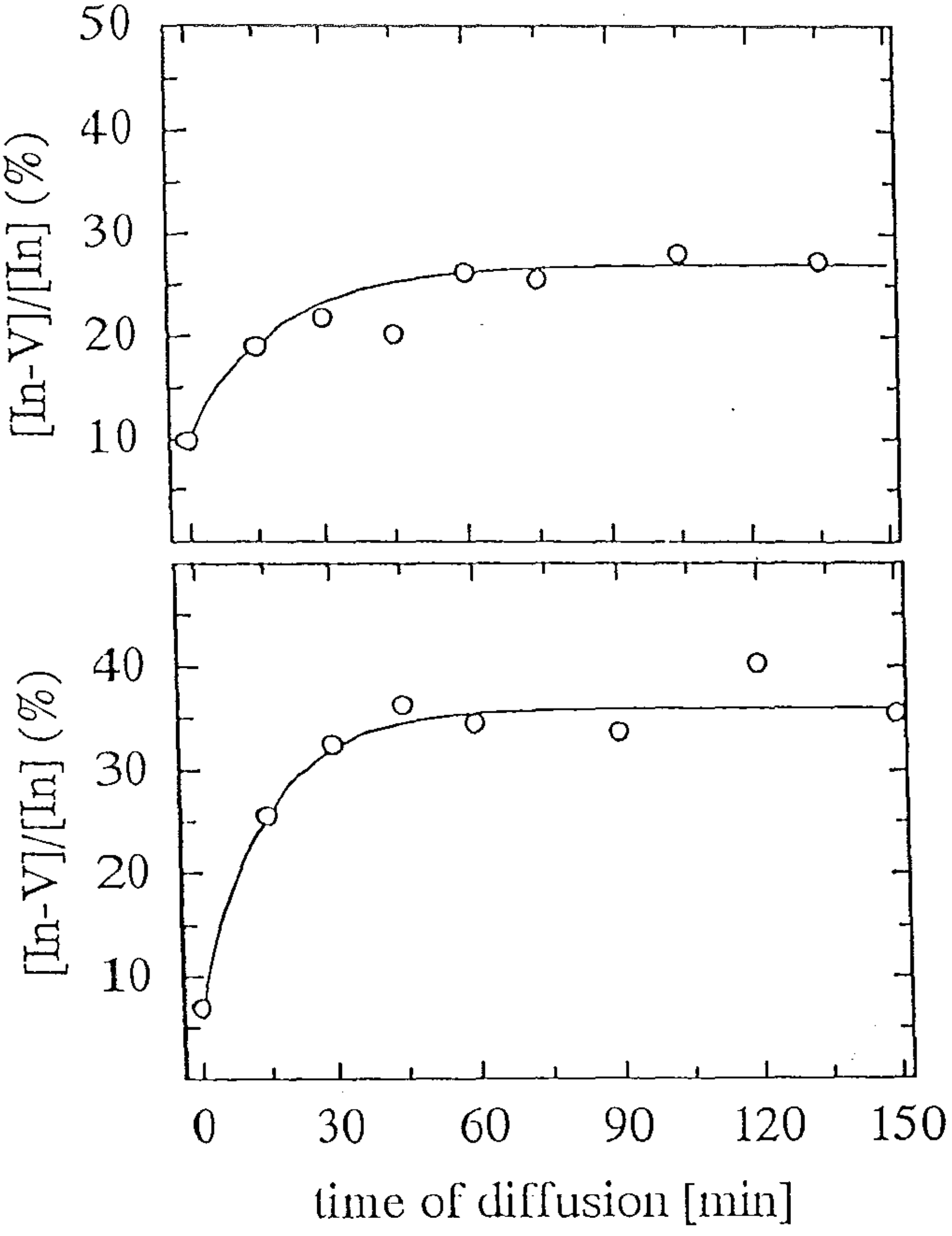

Fig. 4. 15 Results of exp. 5

Lithium isothermal experiments fixing T_{Li} at 500K.

Top: T_{ZnSe} = 650K and

Bottom: T_{ZnSe} = 725K

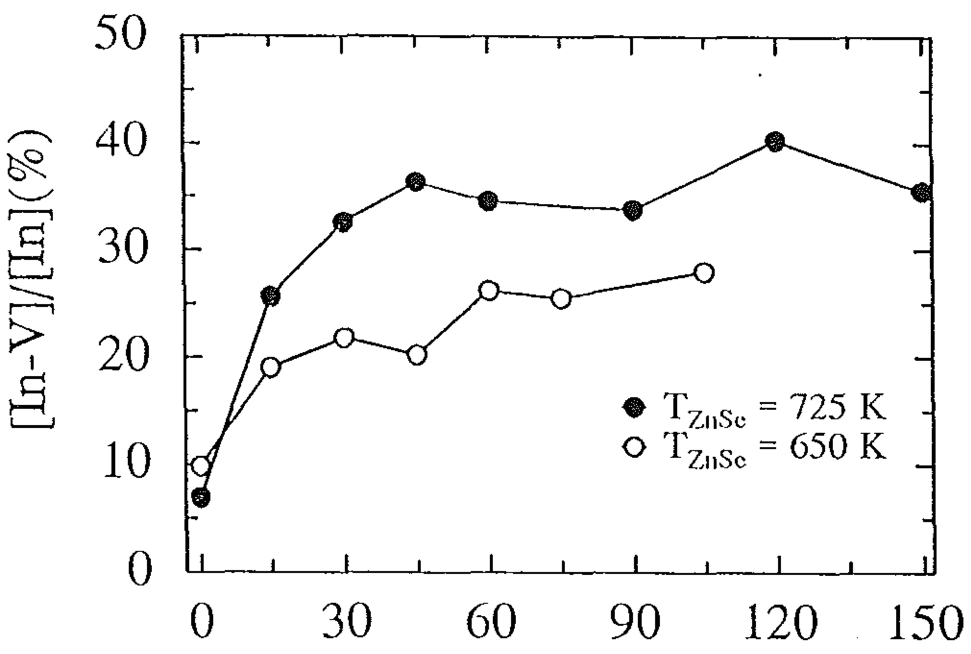

Fig. 4.16 Dependence of the Saturation value for the $In_{Zn} - V_{Zn}$ fraction on the matrix temperature, displaying the difference between the two isothermal experiments for a better comparison

4.13 CONCLUSIONS AND OUTLOOK

1. It is noted from our experimental results that no donor-acceptor pairing of the type In_{Zn} - Li_{Zn} was observed by PAC. In all experiments, the values of the hyperfine parameters specify the same defect: the metal vacancy, V_{Zn} in ZnSe characterized with ν_Q = 72MHz, η = 0.05 and the lattice direction of the EFG (V_{zz}) being along the <111> lattice direction.

2. Lithium doping for the investigated diffusion temperature range has only brought about an increased concentration of the relative fraction of In_{Zn} - V_{Zn} pairs by a factor of 4..

3. As a consequence of our special thermal treatment, it can be concluded that Li induces new vacancies - a new result explaining the enhancement of In_{Zn} - V_{Zn} pairs after Lithium diffusion.

4. The different influences of vapour pressure (T_{Li}) and sample temperature (T_{ZnSe}) were noticed in governing the incorporation of Lithium into ZnSe.

5. The enhanced vacancy creation, [25] observed during Li-incorporation might also shed new light on the problem of the missing p-type conductivity after Li-diffution.

6. These types of experiments should be continued since they could lead to interesting results. Indeed, the vacancy creation following Li-diffusion can as well be investigated using positron annihilation experiments. Moreover, hall effect measurements could also supplement the PAC studies of Lithium doped ZnSe samples.

Appendix A Electric Hyperfine Interaction

In reference to the second term in eq(1) of chapter 3, the electrostatic interaction between a nucleus with charge Ze and the surrounding charges is characterized with the interaction energy:

$$E_{el} = \int \rho_n(\vec{r})\ V(\vec{r})\ d\tau \tag{A1}$$

where $\rho_n(\vec{r})$ is the nuclear charge density at a point having a relative position vector $\vec{r} = x_1\hat{i} + x_2\hat{j} + x_3\hat{k}$ with respect to the center of symmetry of the nuclear charge. $V(\vec{r})$ is the coulomb potential at the same point $\vec{r}$ due to all other charges. $d\tau = dx_1 \cdot dx_2 \cdot dx_3$ represents the volume element.

Choosing the origin of the coordinate system to coincide with the center of symmetry of the nuclear charge, $V(\vec{r})$ can be expanded in a Taylor series at the origin $\vec{r} \equiv 0$, yielding:

$$V(\vec{r}) = V_0 + \sum_{i=1}^{3} \left[\frac{\partial V}{\partial x_i} \right]_0 x_i + \frac{1}{2} \sum_{i,j=1}^{3} \left[\frac{\partial^2 V}{\partial x_i \partial x_j} \right]_0 x_i x_j + \ldots \tag{A2}$$

Upon substituting A2 into A1, we obtain

$$E_{el} = V_0 \int \rho_n(\vec{r}) d\tau + \sum_{i=1}^{3} \left[\frac{\partial V}{\partial x_i} \right]_0 \cdot \int \rho_n(\vec{r}) x_i d\tau +$$

$$\frac{1}{2} \sum_{i,j=1}^{3} \left[\frac{\partial^2 V}{\partial x_i \partial x_j} \right]_0 \cdot \int \rho_n(\vec{r}) x_i x_j d\tau + \ldots \tag{A3}$$

where $\int\rho_n(\vec{r})d\tau = eZ$ is the nuclear charge and it makes the first term in (A3) to be eZV_0. Contained in this term is the electrostatic interaction between the nucleus considered as a point and other charges in the material. It contributes to the potential energy of the crystal as a whole, and it is not interesting for our goal. The electric dipole interaction is expressed by the second term, however symmetry arguments show that it doesnot exist [25]. Higher odd-order terms do not exist for the same reason.

Moreover, even-order terms higher than the third term in (A3) are negligible because their interaction energies are too small to be observed.

Hence, the only term in (A3) which is interesting to us is the third one.

The quantities $(\partial^2V/\partial x_i\partial x_j) = V_{ij}$ form a (3x3) second-rank tensor (eq(3) chapter 3). By a choice of a coordinate system, it is possible to realize that all tensor elements V_{ij} vanish except the diagonal ones, V_{ii}(principal axes system). In so doing, the third term in (A3) can be formulated as

$$E = \frac{1}{2}\sum_{i=1}^{3}V_{ii}\int\rho_n(\vec{r})x_i^2\,d\tau = \frac{1}{2}\sum_{i=1}^{3}V_{ii}\int\rho_n(\vec{r})\left(x_i^2 - \frac{r^2}{3}\right)d\tau$$

$$+\ \frac{1}{6}\sum_{i=1}^{3}V_{ii}\int\rho_n(\vec{r})r^2\,d\tau\ ,\ \text{with } r^2 = \sum_{i=1}^{3}x_i^2 \qquad \text{(A4)}$$

By adding and subtracting the quantity $\frac{1}{6}\sum_{i=1}^{3}V_{ii}\int\rho_n(\vec{r})r^2\,d\tau$ in (A4)

we introduce into the first term the definition of the nuclear quadrupole moment, the diagonal tensor elements of which in the principal axes system are given by

$$Q_{ii} = \int \rho_n(\vec{r}) \left[3x_i^2 - r^2\right] d\tau \tag{A5}$$

The elements of the tensor are generally given by ,

$$Q_{ii} = \int \rho_n(\vec{r}) \; (x_i x_j - \delta_{ij} \; r^2) d\tau \tag{A6}$$

where summation is performed over the repeated indices and δ_{ij} is the kronecker symbol.

In many nuclei the nuclear charge distribution deviates more or less from spherical symmetry; the deviation may change in going from one state of excitation to another.

A measure of the deviation is given by the electric quadrupole moment eQ whose elements are given in (A6)

To see the value of the electrostatic energy in (A4), let us introduce the Laplace differential equation

$$\Delta V + 4\Pi\rho_e = 0 \tag{A7}$$

Applying (A7) in particular at the point $\vec{r} = 0$ (center of symmetry of the nucleus) we obtain

$$(\Delta V)_0 = \left[\sum_{i=1}^{3} V_{ii}\right]_0 = 4\Pi e \; |\psi(0)|^2, \tag{A8}$$

where $\rho_e = -e|\psi(0)|^2$ is the charge density exerted by the surrounding electrons at the nucleus ($\vec{r} = 0$) with $\psi(0)$ being the Schrödinger wave function at $\vec{r} = 0$.

Substituting (A8) into (A4), we get

$$E = \frac{2}{3}\Pi e|\psi(0)|^2 \int \rho_n(\vec{r}) r^2 d\tau + \frac{1}{2}\sum_{i=1}^{3} V_{ii} \int \rho_n(\vec{r}) \left[x_i^2 - \frac{r^2}{3}\right] d\tau \equiv E_I + E_Q \tag{A9}$$

The first term of (A9) represents the electric monopole interaction. It causes a shift of nuclear energy levels. The second term in (A9) represents the electric quadrupole interaction from which the PAC technique extracts sufficient information about defects surrounding probe atoms. It is worthy to notice that this interaction energy will be better resolved for larger values of the EFG and for probes having a large value of quadrupole moment. This conclusion is a direct consequence of the proportionality of E_Q in (A9) to the EFG (V_{11}) and the nuclear quadrupole moment (Q_{11}).

Appendix B Data Analysis

The extraction of the hyperfine interaction parameters is accomplished by fitting the experimentally observed R(t) spectra into the equation $R(t) = A_{22}\left[f\left\{S_0 + \sum_{n=1}^{3} + S_n \cos \omega_n t\right\} + (1-f)\right]$ using a least squares fit method.

Consequently, interesting parameters will be obtained from the measured spectra: the quadrupolar interaction frequency ν_Q eq.(7), the asymmetry parameter η eq (6)and relative fration, f eq.(19) of ^{111}In probe atoms which coupled themselves with the defects is computed using statistical methods. This is analyzed by a computer program and the errors in the above mentioned parameters are computed over the atomic time scales.

It should be attentively noticed that in all experiments presented here a data point just represents one single experimental result. The same experiment is not repeatedly done for the same data point. In this case, the errors are computed over time scales for the same data pointvia comparisons of observed and fitted values before the specific experiment is finished. In other words, it is the time average of the above mentioned parameters that is computed with an error.

In fact, from the statistical nature of the problem, several instantaneous values will be extracted for the above parameters before the completion of a single experiment which takes about 7-8 hours

R E F E R E N C E S

[1] Y.S. Park and B.K.Shin, in *Electroluminescence*, edited by J.I Pankove, Topics in Applied Physics Vol. 17 (Springer, Berlin, 1977) p. 133

[2] P.J. Dean, H. Venghaus, J.C. Pfister, B.Schaub and J.Marine, J. Luminescence 16 (1978) 363

[3] M.A.Haase, H.Cheng, J.M.DePuydt, and J.E .Potts J. Appl. Phys. 67 (1), 1 January 1990

[4] Y. Marfaing, Prog. Crystal Growth Charact. **4** (1981) 317

[5] Th. Wichert, M. Deicher, G. Grübel, R. Keller, N. Schulz, and H. Skudlik, Appl. Phys. A **48** (1989) 59

[6] Characterization of ZnSe and other II–VI Semiconductors by Radioactive Dopants by Th. Wichert, Thomas Krings, and Herbert Wolf Technische Physik Universität des Saarlandes, 66041 Saarbrücken, Germany

[7] N. Achtziger, A. Baurichter, S. Deubler, D. Forkel, H. Plank, M. Puschmann, H. Wolf and W. Wittuhn and R. Helbig, Materials Science Forum **10-12**, 863 (1986)

[8] II–VI Compounds by BRIAN RAY, 1969

[9] Prog. Crystal Growth Charact. 1981, Vol. **4**, pp. 317–343 by Y. Marfaing

[10] F.A. Kroger and H. J. Vink in Solid State Physics, edited by F. Seitz and D. Turnbull (Academic Press Inc., New York, 1956) Vol. III, p. 310[11] R.F. Brebrick, Phys. Chem. Sol. **4**, 190 (1958); 18, 116 (1961)

[12] G. Mandel, Phys. Rev. **134**, A 1073 (1964)

[13] R. Bhargava, J. Cryst. Growth 59, 15 (1982)

[14] B. Tell: J. Appl. Phys. **42**, 2919 (1971)

[15] H.H. Woodbury: J. Appl. Phys. 36, 2287 (1965)

[16] M. Aven: J. Appl. Phy. 38, 4421 (1967)

[17] M.Aven: II-VI Semiconducting Compounds, ed. by D.G. Thomas (Benjamin Publ. Co., Newyork 1967) p.1232

[18] R.W. Jansen and O.F. Sankey, Phys. Rev. B 39, 3192 (1989)

[19] Th. Wichert, E. Recknagel: Microscopic Methods in Metals, ed. by U. Gonser, Topics in Current Physics, Vol. **40** (Springer, Berlin, Meidelberg 1986) p. 317

[20] Diploma Thesis by Uwe Ott,. Universität des Saarlandes, Saarbrücken, May 1993

[21] Th. WICHERT, N. ACHTZIGER, H. METZNER and R. SIEKEMANN Hyperfine Interaction of Defects in Semiconductors, ch.2

[22] M.Sc Thesis by Mesfin Tsige, A.A.U., Physics Department

[23] PAC Study of the Acceptor Li in II-VI Semiconductors by H. Wolf, Th. Krings, U.Ott, U. Hornauer, and Th. Wichert Technische Physik, Universität des Saarlandes, 66041 Saarbrücken, Germany

[24] T. Sasaki, T. Oguchi and H. Katayama-Yoshida, Phy. Rev. B **43**, 9362 (1991)

[25] Philipp Gütlich, Rainer Link and Alfred Trautwein Mössbauer Spectroscopy and Transition Metal Chemistry, 1978 (p. 13–15)

[26] H. Wolf, U.Hornauer, R. Lermen, Yared Endalamaw, Th. Filz Th. Krings, St. Lauer, U.Ott, E. Singer, Mesfin Tsige and Th. Wichert, Metal Vacancies in Li and In doped ZnSe and CdS, 17th international conference on defects in Semiconductors ICDS-17, Gmunden, July 18 - 23 1993, Austria